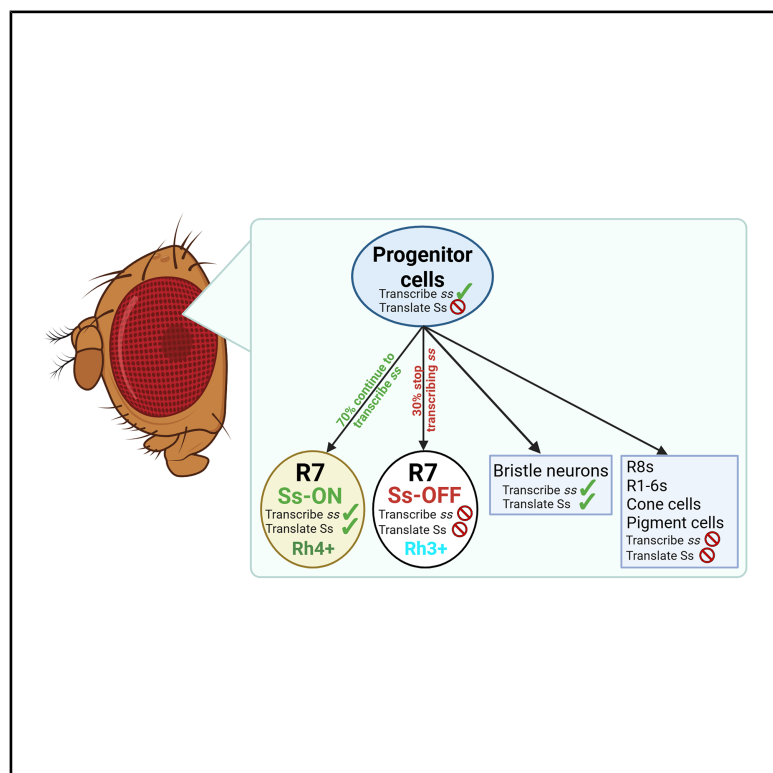# Current Biology

Cell fate ratios are encoded by transcriptional dynamics in the *Drosophila* retina

Graphical abstract

Authors

Julia Ainsworth, Yunchong Zhao,
Ke Gao, ..., Andreas M. Ernst,
Hernan G. Garcia, Michael W. Perry

Correspondence

mwperry@ucsd.edu

In brief

Ainsworth and Zhao et al. show that stochastic patterning decisions in the *Drosophila* retina are made earlier than expected, even before photoreceptor specification, and are controlled by the amount and timing of *spineless* transcription in retina progenitor cells.

Highlights

- Future R7 photoreceptor subtype is determined before R7 specification

- Amount and timing of early *spineless* transcription controls the stochastic ratio

- More continuous early transcription increases the stochastic ratio, and gaps decrease it

- Targeted chromatin opening increases the Ss-ON ratio

CellPress

Current Biology

CellPress

Article

Cell fate ratios are encoded by transcriptional dynamics in the *Drosophila* retina

Julia Ainsworth,[1,8] Yunchong Zhao,[1,8] Ke Gao,[1] Nicholas M. Gravina,[2] Zachary H. Goldberg,[1] Coleman Pinkerton,[1] Scott A. Rifkin,[3] Andreas M. Ernst,[1] Hernan G. Garcia,[2,4,5,6,7] and Michael W. Perry[1,9,*]

[1]Department of Cell and Developmental Biology, School of Biological Sciences, University of California, San Diego, La Jolla, CA 92093, USA
[2]Department of Physics, University of California, Berkeley, Berkeley, CA 94720, USA
[3]Department of Ecology, Behavior, and Evolution, School of Biological Sciences, University of California, San Diego, La Jolla, CA 92093, USA
[4]Department of Molecular and Cell Biology, University of California, Berkeley, Berkeley, CA 94720, USA
[5]Biophysics Graduate Group, University of California, Berkeley, Berkeley, CA 94720, USA
[6]Institute for Quantitative Biosciences (QB3), University of California, Berkeley, Berkeley, CA 94720, USA
[7]Chan Zuckerberg Biohub, San Francisco, San Francisco, CA 94158, USA
[8]These authors contributed equally
[9]Lead contact
*Correspondence: mwperry@ucsd.edu
https://doi.org/10.1016/j.cub.2025.05.037

SUMMARY

Although transcription happens in bursts, it is unclear whether variation in the rate and pattern of bursting matters during animal development. We examined whether the amount and timing of transcription influence the ratio of cell types produced during stochastic patterning of the *Drosophila* retina. This system is balanced between 2 outcomes: ~70% of R7 photoreceptors (PRs) express Rhodopsin 4 (Rh4), and the rest express Rhodopsin 3 (Rh3). Cell fate depends on the cell-intrinsic binary decision to express the transcription factor *spineless* (Ss). Changing the *ss* bursting pattern by replacing the *ss* core promoter led to a different ratio of R7 PR types. We hypothesized that random variation in the timing of transcriptional initiation followed by autoregulation might control the outcome. Instead, we found that the decision occurs before R7 specification and before protein is made, with no feedback via Ss protein. Surprisingly, this happens in a field of progenitor cells that give rise to all retina cell types, which all initially transcribe *ss*. A subset stops transcribing *ss* over time. Those that become R7s and maintain *ss* transcription take the Ss-ON/Rh4 fate. Live imaging of *ss* transcription suggests increased time spent in off periods could decrease the probability of new transcription and therefore the Ss-ON ratio. Transiently increasing continuity of transcription produces all Ss-ON outcomes, while introducing longer gaps lowers the ratio. Targeting CBP to the *ss* locus increases the ratio, indicating a repressive role for chromatin state during periods when transcription is inactive. We conclude the ratio is set by the amount and dynamics of *ss* transcription.

INTRODUCTION

During development, different genes exhibit different transcriptional dynamics over time.[1–7] Gene regulatory features such as promoter type,[8–12] chromatin conformation and state,[13–17] tethering elements,[17] and the number of overlapping or shadow enhancers[8,18–20] can influence the rate and dynamics of transcription. These dynamics include the duration of periods of active transcription, intervals between active periods, and the dynamics of RNA polymerase loading within active periods. Whether variability in transcriptional bursting dynamics is important for developmental outcomes has been the subject of debate. Some studies have shown that the uniformity of transcriptional initiation is critical for pattern formation in development.[9] Others have found that variable dynamics can be averaged out over time by the accumulation of stable mRNA or via diffusion of the protein produced between neighboring cells.[21,22] These studies have focused primarily on the *Drosophila* embryo,

where live imaging tools such as the MS2 and PP7 systems have enabled visualization of gene expression dynamics over time. However, *Drosophila* embryo development is robust to perturbation[8,23] and temporally distant from terminal cell fate decisions, making it difficult to connect differing transcriptional dynamics and subtle changes in gene expression to phenotypic consequences and organismal fitness. The extent and contexts in which these dynamics matter during development are largely unknown.

One context in which variation in transcriptional bursting may be especially relevant is during stochastic cell fate specification. In many cases, cell fate specification events are highly reproducible and essentially deterministic, with minimal variability. In other cases, inherent variation can be used to produce divergent fates. For example, an elegant and now classic experiment showed that clonally identical bacteria can respond at significantly different rates to the uniform addition of a substrate.[24] Such diversity of response may be beneficial to bacteria in

varying environments.[25–27] This work inspired similar approaches in studying the role of stochasticity in multicellular animal development.[26,28] For example, in the mouse olfactory system, each olfactory sensory neuron stochastically selects a single allele to express from among a cluster of odorant receptor genes.[29] Further, during T cell lineage commitment, the locus *Bcl11b* is irreversibly but stochastically activated at different times in identical cells due to an epigenetic switch.[30] Thus, in an increasing number of multicellular contexts, stochastic patterning is thought to utilize subtle random variations in a purposeful way to help diversify the number and distribution of cell types during development. However, the source of useful variation is often unknown, as are the mechanisms that amplify initially slight differences into discrete on/off outcomes in reproducible ratios.

The *Drosophila* retina has become a premier model for the study of stochastic cell fate specification.[28,31–34] In the adult fly, the retina consists of a repeated pattern of unit eyes, called ommatidia, each of which contains 8 photoreceptors (PRs) that express light-sensitive rhodopsin (Rh) proteins. R7 PRs express either Rh4 or Rh3 and are used for color comparisons. The decision of which fate to take and which Rh is expressed is controlled by whether the transcription factor Ss is expressed[35] (Figure 1A). This decision is cell-intrinsic and random and yet produces reliable proportions: each wild-type retina contains ~70% Rh4-expressing and ~30% Rh3-expressing R7s, but the pattern of each fly's retina is different, like a human fingerprint. As in human retinas, the PRs also form a random, stochastic mosaic.[32] Ss protein first appears in the L3 larval eye imaginal disc in a subset of R7 PRs after they are initially specified (Figure 1A, left, R7s indicated with white dashed circles, Figure S1A). At this stage, levels of Ss expression are very low. Protein expression strengthens by mid-pupation 2 days later (Figure 1A, middle). Rh expression downstream of Ss does not begin until just before eclosion, ~96 h after pupation (Figure 1A, right). The decision of whether to express Ss controls R7 PR subtype, subsequent signaling to the neighboring R8 cell, and the fate of individual ommatidia and which wavelengths they detect.[36–40] In this work, we investigate how otherwise identical retina cells diverge in fate with a particular probability, at what point this decision is made, and what factors influence the ratio of cell types produced.

A recent study identified a regulatory region ~5 kb upstream of the *ss* promoter that drives *ss* transcription in a stripe in the eye disc near the morphogenetic furrow (MF), close to where PR patterning is initiated.[45] Deletion of this enhancer resulted in fully Ss-OFF adult retinas, suggesting that early *ss* expression is important for the stochastic choice. They next tested global chromatin modifications and concluded that chromatin state is important, either directly or indirectly, for the stochastic decision.[45] The authors proposed a model of how transcription might oppose chromatin state in generating the stochastic choice, but this model has not been directly tested.

Here, we employ live imaging of transcription,[1,46,47] genetic modification of the *ss* locus, and targeted deactivated or "dead" Cas9 (dCas9) fusions[48,49] to examine how transcriptional dynamics affect stochastic cell fate specification in R7 PRs. We present evidence that changing the pattern of transcription over time results in the production of different ratios of cell and

ommatidial types and that the continuity of transcription in an early period of expression controls the final ratio. This early decision happens independently of levels of Ss protein, which we show does not influence the probability of transcription. We find that longer gaps between periods of active transcription lead to more cells taking the Ss-OFF fate, while more continuous transcription in this period increases the ratio of Ss-ON R7s. This in turn controls the ratio of PRs that express different Rhs and therefore determines which color comparisons are made. We hypothesized that chromatin state might oppose transcriptional activation. In this model, methylation or deacetylation occurs during gaps in transcription. Longer gaps, which occur by chance, lead to correspondingly larger decreases in accessibility, leading to a lower probability of new transcription. This would provide a mechanism by which initially slight differences could be amplified into producing a fully Ss-OFF state in a subset of cells. We tested this model by targeting the chromatin opener dCas9-CBP to the *ss* locus and observed an increase in the final Ss-ON ratio, implicating chromatin state as the negative regulator. Together, our results suggest that the pattern of transcriptional bursting controls the ratio of cell types produced.

RESULTS

Previous studies have suggested that transcriptional synchrony can be essential for coordinating cell behavior[9] and that transcription is inherently noisy.[50] These observations raise the possibility that transcription might provide a useful source of variability when the goal is to produce divergent outcomes during stochastic cell fate specification. We first set out to test whether differing patterns of transcriptional bursting influence the ratio of cell types produced.

Modification of the *ss* core promoter produces different transcriptional bursting dynamics

Previous studies indicate that properties of the core promoter, such as whether it is paused or non-paused, can influence synchrony of transcriptional initiation and bursting dynamics over time.[9,10] We used CRISPR-Cas9 homology-directed repair[51] to seamlessly replace 120 base pairs of the endogenous *ss* core promoter with a core promoter of similar size from the *snail* locus (diagram in Figure 1B, sequence in Table S1). Properties of a set of promoters, including *snail*, had been evaluated previously in the embryo.[9,10] This modification is homozygous viable and showed no defects in antennal, leg, or bristle patterning as might be expected for disrupted Ss expression in these tissues, indicating the functionality of the new promoter in this context (Figures S1B and S1C). We then evaluated whether promoter modification produces corresponding changes in *ss* transcriptional bursting dynamics.

We used live imaging of transcription to evaluate whether the *spineless-snail* promoter-swap line exhibits modified patterns of transcriptional bursting. We first developed new fly lines to make *in vivo* movies of transcription in developing eye discs by adapting the MS2 system.[46] While MS2 has become well established in the *Drosophila* embryo,[1,2,17] it has not previously been used to visualize transcriptional dynamics in other *Drosophila* tissues. We created UAS-MS2 coat protein-GFP (MCP-GFP) fly lines, identified appropriate GAL4 drivers, and optimized a live imaging
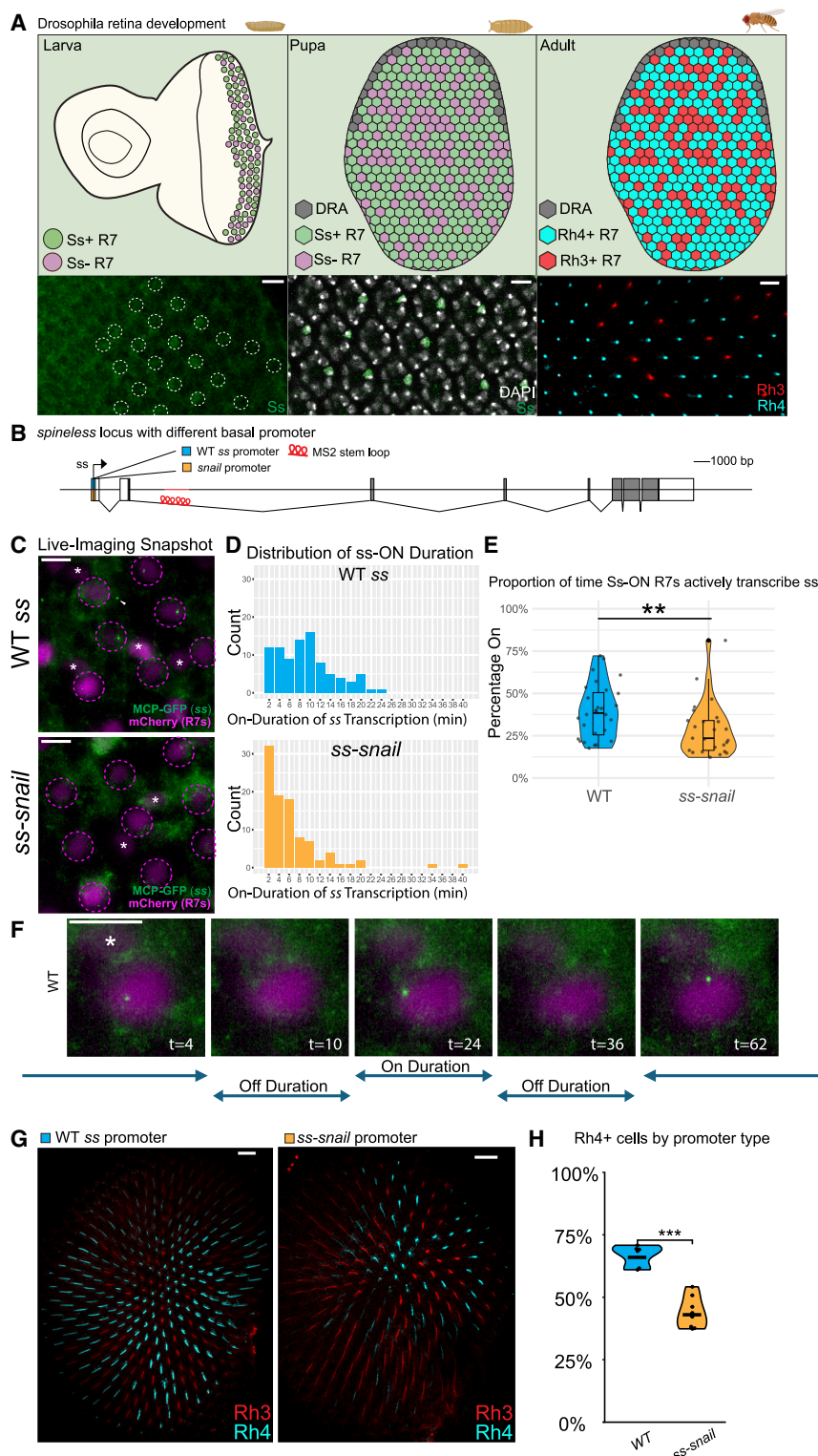
Current Biology
Article

CellPress

Figure 1. Promoter replacement produces different patterns of transcriptional bursting and ratios of cell types

(A) Drosophila retina development at larval, pupal, and adult stages as illustrations (top) and immunohistochemistry (IHC) stains (bottom). The earliest Ss protein detected in the eye disc begins in a subset of R7 PRs at L3 stage (left, Ss in green, R7s identified by white dashed circles). Expression strengthens by 50% pupation (P50) in a stochastic subset of R7s (middle). Ss expression controls adult Rh expression in R7 PRs[35,41–43], where Ss-ON R7s express Rh4 (cyan) and Ss-OFF express Rh3 (red). The dorsal rim area (DRA) is patterned via a different mechanism.[44] R7 positions identified via counterstain (see Figure S1A). Partly created using Biorender.com. Scale bars from left to right: 5, 10, and 10 µm.

(B) Schematic showing a modified *ss* locus containing 24MS2 stem-loop repeats (shown as red loops) and the snail core promoter swapped in place of the endogenous core promoter.

(C) Single frame taken from MS2 live imaging experiments of L3 eye discs showing R7 cells (dashed magenta circles) in control (top) vs. *ss-snail* (bottom). Magenta, PM181-mCherry (R7 marker); green, MCP-GFP. Asterisks, PM181-mCherry-expressing cone cells. Arrowhead, cone cell *ss* transcription (excluded from quantification). Scale bar: 5 µm.

(D) Distribution of *ss*-ON intervals (min) in WT (top panel, n = 90) and *ss-snail* (bottom panel, n = 96). Wilcoxon rank-sum test with continuity correction; p = 6.938 × 10⁻⁶.

(E) Violin and box plot of data plotted in (F) but grouped by each cell measured, where each data point defines what percentage of the observation time each cell was observed to be "on" or transcribing *ss*. A Wilcoxon rank-sum test with continuity correction was used to compare genotypes, p = 0.00752.

(F) Still frames of an example of late L3 R7 turning *ss* on/off over time. Illustration below shows how on/off periods of *ss* were recorded. Asterisk, cone cell. Scale bar: 5 µm. Time (t) refers to min elapsed since the movie began.

(G) IHC of Rh3 and Rh4 in representative WT (left) and *ss-snail* (right). Scale bar, 20 µm.

(H) Different R7 ratios are obtained when the *ss* promoter is replaced; ***p < 0.001. Spineless WT promoter: n = 6 retinas, 1,439 total ommatidia; snail promoter: n = 8 retinas, 2,242 total ommatidia. Wilcoxon rank-sum test, p = 5.61 × 10⁻⁶.

See also Figure S1; Tables S1, S2, and S4; Videos S1 and S2; and Data S1.

protocol (see STAR Methods). We used CRISPR-Cas9 genome editing to insert 24 copies of the MS2 reporter sequence into the 5' end of the second intron of endogenous *ss* (Figure 1B), allowing us to visualize nascent *ss* transcription in live, developing eye discs.

We imaged *ss* transcription *in vivo* in R7 PRs in whole-mounted control *ss*-wild type (WT) and *ss-snail* late larval eye discs (Figures 1C–1F; Data S1). To identify R7 nuclei in live imaging experiments, we constructed a fly line containing PM181-mCherry-NLS (Figure 1C). PM181 is a set of multimerized

elements derived from an enhancer within *sevenless*,[52,53] which drives expression in most R7s (dashed circles) and exhibits leaky expression in a small number of cone cells (asterisks), which can be identified by position and shape. Figure 1C shows frames taken from movies of *ss* transcription in each background (Videos S1 and S2). Accumulation of MCP-GFP onto 24 × MS2 stem loops produces small green dots, which indicate sites of active *ss* transcription. The movies were examined in Fiji/ ImageJ to identify and track individual on and off *ss* transcription events (example tracking in Figures 1F and S1E). We focused on the duration of "*ss+*" and "*ss−*" periods and not dynamics within *ss+* periods (as in Bothma et al.[2]). We compared all measured *ss+/−* event durations (Figure 1F) and *ss−* intervals (Figure S1E) between WT ($n = 90$, 2 movies) and *ss-snail* ($n = 96$, 5 movies) backgrounds. We found that R7s in the *ss-snail* promoter-swap background transcribe *ss* in on-periods that are of significantly shorter duration compared with WT (Wilcoxon rank-sum test with continuity correction, $p = 6.938 \times 10^{-6}$). WT R7s also spend a higher proportion of the time actively transcribing than *ss-snail* (Figure 1E, Wilcoxon rank-sum test with continuity correction, $p = 7.519 \times 10^{-3}$). In these plots, each data point represents the percentage of time an R7 cell exhibits *ss* transcription. These results indicate that the change in promoter successfully generated different transcriptional dynamics over time.

Promoter modification leads to the production of different cell fate ratios

Next, we quantified the ratio of Ss-ON, Rh4+ R7 cells to Ss-OFF, Rh3+ R7 cells in adult flies homozygous for the promoter-swap at the *ss* locus to determine the effect on cell fate outcomes (Figures 1G and 1H). We observed a 35% decrease in Ss-ON ratio as reported by Rh expression (fraction of Rh4+ R7s, $p = 5.61 \times 10^{-6}$) (Figure 1H). A corresponding difference was observed in pupal retinas, with a lower proportion of *ss*-transcribing R7s observed in *ss-snail* compared with WT ($p = 0.0143$, Figures S2A and S2B). The observed P50 *ss*-ON/OFF ratio marked by Ss-ON reporter Dpr11[54] (Figure S2C) is not significantly different from the adult Rh ratios observed in both *ss-snail* and WT backgrounds (Figure S2D). Thus, our experimental modification of transcriptional dynamics also produces a different ratio of ommatidial types. We next sought to determine how different dynamics of transcription are connected to the ratio of cell types produced.

Transcription factor autoregulation does not influence cell type ratios

Direct or indirect autoregulation are common mechanisms used to provide feedback in gene regulation. Studies in other contexts have demonstrated that feedback is required to amplify initial, slight variations between cells to produce fully divergent, binary on/off outcomes.[55,56] We hypothesized that the earliest cells to begin *ss* transcription might be more likely to become Ss-ON through autoregulation, with earlier feedback increasing the probability of additional transcription. In this scenario, differences in the timing of initial gene expression would play a role in determining which cells ultimately became Ss-ON vs. Ss-OFF. We hypothesize that feedback at the protein level could play this role and tested whether autoregulation is involved in establishing fully ON/OFF fates and divergent outcomes.

We used Ss overexpression (Figures 2A–2D) and an Ss null mutant (Figures 2E–2G) to examine the probability of transcription of the endogenous *ss* locus in the presence of additional Ss protein or when Ss protein is missing. We expected that the transient addition of Ss protein in recently recruited PRs in L3 would produce a change in adult Rh ratios. If Ss protein provides positive feedback, more R7 cells should take the Ss-ON fate. We therefore transiently expressed Ss using the GAL4/UAS system, with either PM181-GAL4 (Figure S2E) or lGMR-GAL4, a strong driver in all PRs (Figure S2F), in the presence of GAL80ts, a temperature-sensitive repressor of GAL4. Early L3 larvae were shifted to 29C (permissive temperature, GAL80ts non-functional) for 12 h of Ss expression and then returned to 18C to block further GAL4-driven expression (time course shown in Figure 2A). Counter to our prediction, this had no effect on the final phenotype, and R7 Rh ratios were not significantly different (Figure 2D, $p = 0.271$).

In parallel, we used hybridization chain reaction (HCR) RNA *in situ*[57] to examine the effect of Ss overexpression and observed no significant difference in the probability of transcription of the endogenous *ss* locus at L3 stages (Figures 2B and 2C; $p = 0.758$). We used an RNA probe set targeting *ss* introns to specifically detect and label nascent, unspliced transcripts from the endogenous locus and not the intron-less ectopic UAS-*ss* mRNA (Figure 2B) and quantified the fraction of R7s exhibiting active *ss* transcription (Figure 2C). These results suggest that the addition of Ss protein does not influence the probability of transcribing the endogenous *ss* locus.

Next, we examined *ss* mutants using an *ss* null allele. Because this mutation is early lethal when homozygous, we used a genetic method for making whole mutant eyes, as in Duncan et al.[58] and Wernet et al.[44] Surprisingly, no decrease in the number of sites of active *ss* transcription was observed at pupal stages (Figures 2E–2G). This allele has been characterized as a null mutation[44,58] and results in loss of Rh4-expressing R7s (confirmed in Figure 2G). In the absence of functional Ss protein, the native *ss* locus is still transcribed in the same fraction of R7 nuclei as in WT (Figure 2E, $p = 0.232$). We conclude that the probability of *ss* transcription does not depend on functional Ss protein, suggesting that Ss protein is not the source of feedback that acts on initial variability to produce fully on or off outcomes. We next sought to directly visualize initial transcription and whether timing of initiation might correlate with the on/off decision.

The stochastic decision is made earlier than expected

We used the MS2 system to visualize *ss* transcription in the L3 eye disc over time to look for connections between the timing and patterns of transcriptional activity and cells that take ss-ON vs. OFF fates (Figures 3A–3F). Figure 3B shows still frames at 0, 30, and 60 min from a movie visualizing *ss* expression (Video S3), with MCP-GFP shown in green at sites of active transcription. The fraction of R7s that actively transcribe *ss* at a given moment is plotted over time and compared with the cumulative fraction of R7s that have been or are currently active (Figure 3C). The fraction of R7s that actively transcribe *ss* remains near 30%, similar to the fraction observed in fixed-tissue stains (Figure 2C). The PM181-mCherry R7 marker is not 100% penetrant, and

Current Biology
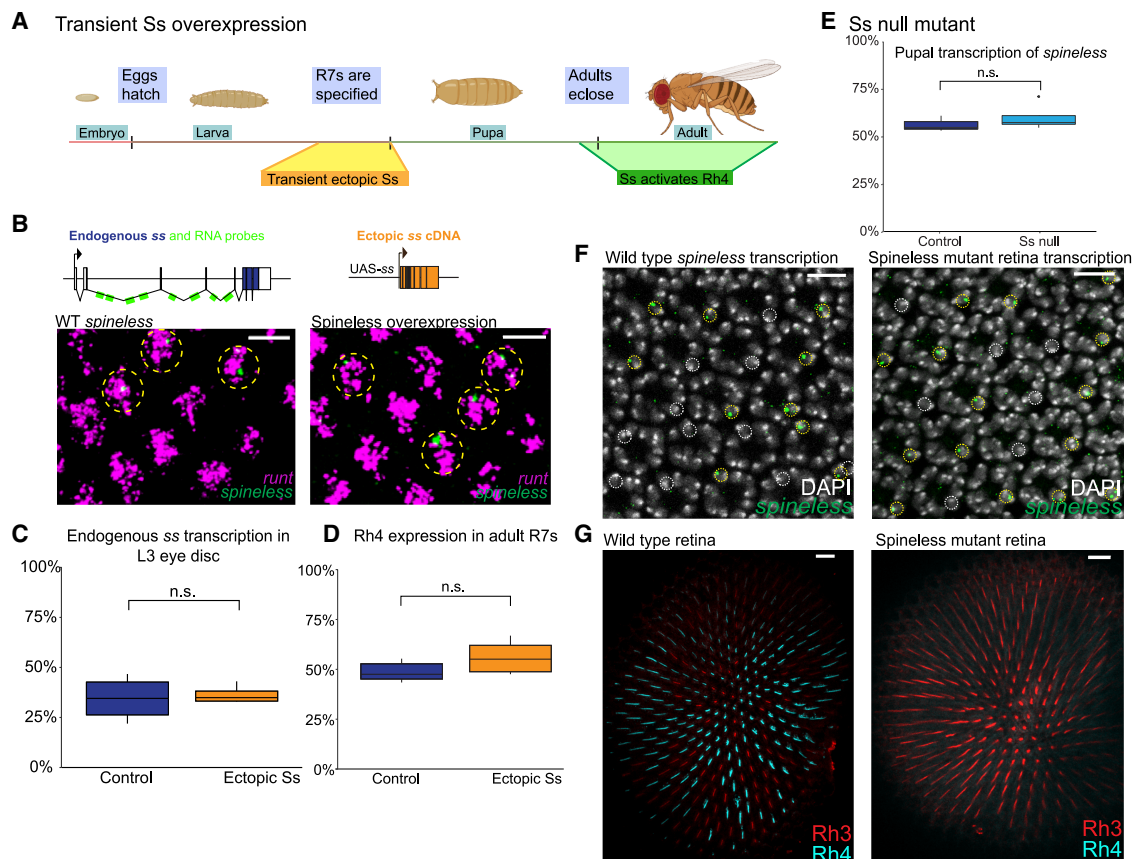## Article

🔹 **CellPress**

Figure 2. Autoregulation does not influence cell type ratios

(A) Timeline of Ss overexpression. Orange box indicates when Ss was transiently expressed. Created with Biorender.com.

(B) Transient Ss overexpression: intronic HCR *in situ* probes bind endogenous *ss* introns but not ectopic UAS-Ss, which lacks introns. Example HCR images are shown for WT and Ss overexpression backgrounds (driven by PM181-Gal4). Runt in magenta and *ss* in green; quantified in (C). Scale bar, 5 μm.

(C) Comparison of the probability of *ss* transcription in L3 eye discs in control vs. Ss overexpression. The fraction of R7s that actively transcribe the *ss* locus is quantified in control with an average of 34.44% Ss-ON ($n = 4$ discs; 506 ommatidia) vs. transient Ss overexpression using UAS-Ss with an average of 36.44% Ss-ON ($n = 4$ discs; 591 ommatidia). The fraction active is not significantly different, $p = 0.758$, two-tailed independent t test.

(D) Comparison of adult R7 Rh ratios in control vs. transient Ss overexpression. Quantification of R7 Rh ratios in adult retinas ($n = 6$; 1,679 total ommatidia) vs. flies of the same genotype kept at permissive temperatures for Ss overexpression during a 12 h window beginning in L3 (shown as orange bar; $n = 4$; 1,598 total ommatidia) produces R7 Rh ratios that are not significantly different. $p = 0.271$, two-tailed independent t test.

(E) Comparison of the fraction of R7 PRs that actively transcribe the *ss* locus in control ($n = 3$; 344 total ommatidia) vs. Ss null mutant background ($n = 4$; 471 total ommatidia). The fraction is not significantly lower than controls, $p = 0.232$, one-tailed independent t test.

(F) HCR *in situ* hybridization of pupal retinas showing *ss* transcription in a WT control (left) vs. Ss null mutant (right), quantified for the fraction active in (E). Yellow dashed circles indicate R7s with active sites of *ss* transcription, while white circles indicate inactive R7s. Scale bar, 10 μm.

(G) Left: WT adult retina with stochastic expression of Rh3 and Rh4. Right: Ss null mutant adult retina with 100% Rh3 expression. Scale bar, 20 μm. n.s. not significant, *$p < 0.05$, **$p < 0.01$, ***$p < 0.001$.

See also Figure S2 and Table S2.

some R7s, which can be identified by shape and position, are unlabeled (arrowheads in Figure 2C). Cone cells, which are identified by position, shape, and lack of R7 marker staining, also occasionally show transcription of *ss* (arrows, Figure 3B). The cumulative fraction of R7s that express *ss* plateaus at 70%, with all "*ss*-ON" R7s exhibiting one or more bursts by 65 min. Unexpectedly, the remaining 30% of newly specified R7s are never observed to express *ss* (cells circled in white). This suggests that these cells have already made the decision to become *ss*-OFF even before they are specified as R7s. We observed R7s in the *ss*-ON subset that already transcribe *ss* before the R7 reporter first turns on (Video S3). Looking deeper into the tissue in fixed samples, we observed sites of active *ss* transcription in many cells that have not yet been recruited as future retina cell types (Figures 3E and S3A). This was unexpected because Ss protein has not been observed in these undifferentiated cells (Figure 3D). Together, these observations suggest that the decision of whether or not to transcribe *ss* occurs even before R7 recruitment.

In parallel, we used fixed-tissue imaging of HCR *in situ* to visualize *ss* mRNA at sites of nascent transcription (using intronic probes) and mRNA accumulation (using exonic probes) in late L3 retinas (Figures 3E and S3A). Little to no exonic *ss* mRNA was detected outside sites of transcription (Figure S3A),
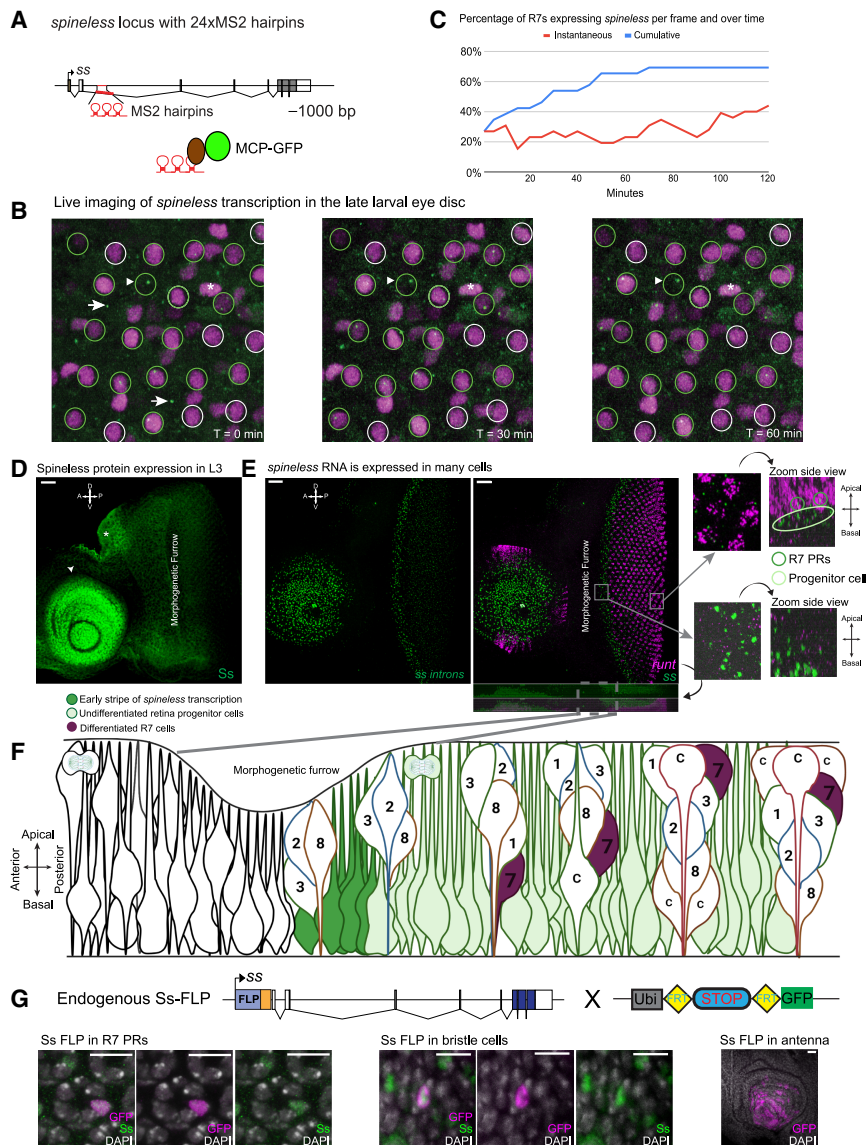
Figure 3. The stochastic decision is made in retina progenitor cells, which do not express Ss protein

(A) Diagram of the *ss* locus showing 24 copies of the MS2 stem-loop reporter inserted into an intron of the spineless gene and a schematic showing the MCP-GFP protein bound to mRNA.

(B) Individual frames from an MS2 movie used to live image *ss* transcription at times = 0, 30, and 60 min. R7 PRs are circled in white (ss-OFF) or green (ss-ON). An R7 reporter PM181-mCherry is shown in magenta, and MCP-GFP is shown in green. The R7 reporter is not fully penetrant such that some R7s are not labeled (arrowhead) and some non-R7s cone cells are labeled (asterisk). Arrows show cone cell *ss* transcription (excluded from quantification).

(C) Quantification of the fraction of R7s that express *ss* in the MS2 movie shown in (B) over time. The red line shows the fraction active in each frame ("instantaneous"), and the blue line shows the cumulative total of active R7s.

(D) Ss antibody stain of an L3 eye-antennal disc. Arrowhead, antennal disc; asterisk, region of future ocellus. Scale bar, 20 μm.

(E) HCR *in situ* hybridization for *ss* and runt, with a view of the z axis (side view) below. Left, intronic *ss* expression (green). Right, same image with both intronic *ss* and runt (magenta). Runt expression marks R7 and R8 PRs. At right, zoomed insets are shown with corresponding side views in the early stripe pattern and specified R7s, where R7 nuclei (marked by runt) can be seen apical to more basal retina progenitor cell nuclei and sites of *ss* transcription. The side panel showing R7 nuclei from the top includes only apical slices to show only R7-containing sections. Scale bar, 20 μm.

(F) Schematic of a side view of a larval eye disc during PR recruitment. Transcription of *ss*, indicated in green, begins in an early stripe pattern near the MF in cells with basal cell bodies. Expression continues in more posterior cells but with lower levels of transcription. A subset of cells from this basally located retina "progenitor pool" are recruited via sequential rounds of signaling into the future retina[59] and move apically. Newly differentiate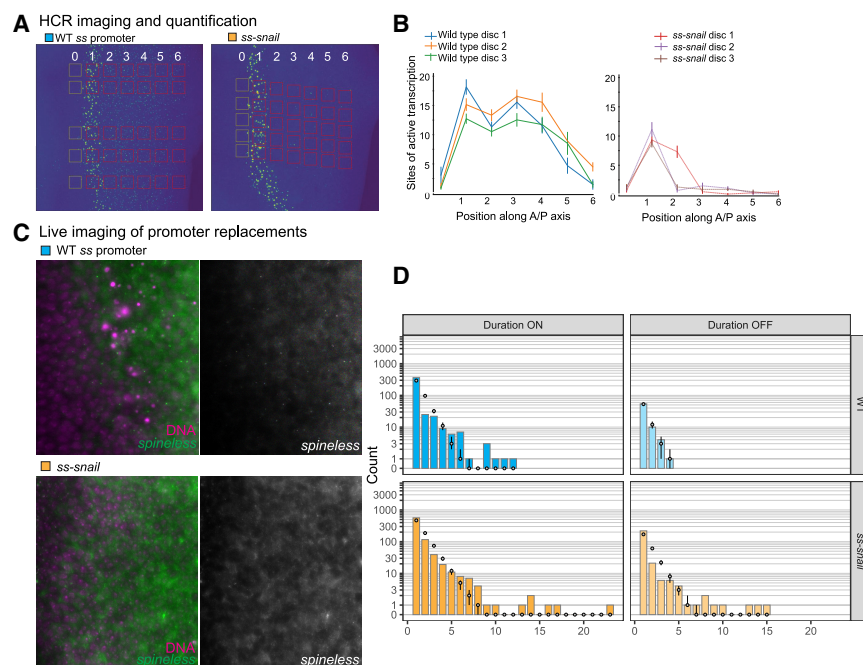d R7s that begin to express runt and other R7s markers are shown in magenta. Numbers correspond to PR number and (C) indicates cone cells. Modified from Ready.[60]

(G) Ss-flp labels R7s, bristle cells (middle), and antennal disc cells (right). No R8 or outer PRs were labeled. R7s were determined based on position and expression of Spalt (Figure S3). Scale bar, R7 and bristle cells, 10 μm, antenna, 20 μm.

See also Figure S3; Tables S2 and S4; and Video S3.

indicating rapid degradation compared with the mRNAs of other genes such as the R7+R8 marker *runt*, which was observed both at sites of transcription and accumulating in the cytoplasm (Figures 3E and S3A). *ss* is transcribed in a narrow dorsal-ventral stripe of cells as they leave the MF as well as in a pool of potential retina progenitor cells from which PRs and other retina cell types are recruited (Figure 3E; side-view schematic in Figure 3F). These cells have basal nuclei and cell bodies, which move apically during the process of recruitment and specification. The anterior-posterior axis can be used as a surrogate for time in the patterning process, with the furrow progressing from posterior to anterior (right to left), leaving increasingly differentiated cells in its wake (Roignant et al.[59]). Many cells of the retina progenitor pool are not recruited and later die during targeted cell death in pupal stages.[59] Magnified views of the early *ss* stripe pattern reveal that all or nearly all cells in this region actively transcribe *ss* in fixed snapshots, far more than the 70% that transcribe ss at R7 recruitment (Figure S3B). This suggests that all retina progenitor cells express *ss* prior to fate specification, a conclusion also supported by a previous study.[45]

Early *ss* transcription does not lead to Ss protein production

The relatively high fraction of cells exhibiting active transcription, as visualized by HCR, contrasts with protein production, as visualized by antibody stain (compare Figures 3D, 3E, and S3A). We observed high levels of Ss protein in the antennal disc (Figure 3D, arrowhead) and lower levels of Ss in the anterior corner of the eye

Current Biology
Article

CellPress

Figure 4. Different patterns of transcriptional bursting result in differing cell type ratios

(A) Heatmaps of HCR *in situ* hybridization in L3 eye discs labeled with probes targeting intronic *ss* mRNAs. Signal is present at sites of active transcription in WT vs. *ss*-snail. Sites of transcription within marked red squares are quantified at seven positions on the anterior/posterior (A/P) axis in (B).

(B) Quantification of the number of sites of active transcription at positions on the A/P axis in control vs. *ss*-snail. Error bars represent the distribution of values measured at different dorsal-ventral positions in each sample.

(C) Single frames taken from MS2 live imaging experiments in the retina progenitor cells in control (top) vs. *ss*-snail (bottom). Sir-DNA, a live DNA dye (magenta), and MCP-GFP (green) quantified in (D).

(D) Quantification of *ss* burst duration (left) and off-interval (right) in control (top) vs. snail promoter-swap lines (bottom). *ss*-WT promoter (top left), 1.491 min average trajectory length (stdev = 1.425), 438 total detections; 69 total off-intervals (top right), 1.304 min average trajectory off time (stdev = 0.644), maximum off time measured of 4 min (top right). *ss*-snail (bottom left), 776 total detections, 1.661 min average trajectory length (stdev = 1.803); 265 total off-intervals (bottom right), 1.491 min average off time (stdev = 1.427), maximum off time of 15 min. *ss*-snail is significantly more skewed than WT ($p = 3.58 \times 10^{-2}$). The gray dots mark the medians of the posterior distributions of counts for each duration given the data and the assumption of a Poisson process. The surrounding black lines indicate 95% highest density intervals for the posterior distributions (posterior predictive *p* values: $WT_{ON} = 0.0011$; $WT_{OFF} = 0.672$; *ss*-snail$_{ON} < 0.0001$; *ss*-snail$_{OFF} = 0.0001$; see STAR Methods for details).

See also Figure S4, Tables S1, S2, and S4, and Videos S4 and S5.

disc near where the ocelli will form (Figure 3D, asterisk). Faint Ss staining can be seen in a subset of the oldest R7s in the most posterior positions (Figure 1A). We did not observe specific antibody staining in early stripe or retina progenitor cells despite their strong transcription of *ss*. To test whether a faint antibody signal comes from low amounts of Ss protein or from non-specific binding, we made labeled Ss null mutant clones that allow us to compare adjacent regions with or without Ss protein present (Figures S3C and S3D). We observed no difference in weak antibody signal in this region in retina clones, despite a clear reduction of signal in antennal clones, indicating that the weak signal in stripe and progenitor cell regions is non-specific.

As an alternate way to detect whether Ss protein is present, we used a genetic method to report the history of past Ss expression and again found no evidence that Ss protein is produced in retina progenitor cells. In this "memory cassette" approach, we used CRISPR-Cas9 genome editing to tag the Ss locus with flippase at the N-terminal end, yielding FLP-T2A-Ss (Figure 3G). We then crossed this Ss-FLP construct to flies containing Ubi-FRT-STOP-FRT-GFP[61] to permanently label cells that produce Ss protein. Only a subset of cells "flip" out the stop cassette and express the GFP reporter in each retina. We observed GFP signal in the same cell types in which Ss protein can be seen by immunohistochemistry, such as R7s, antennal cells, and bristle cells (Figures 3G, S3A–S3C, S3E, and S3F), but observed no GFP flipping events in outer PRs, R8s, or pigment cells, all of which are recruited from the same pool of *ss*-transcribing progenitor cells (15 discs, >9,000 outer PRs examined). Combined, these results indicate that *ss* transcription begins even before R7 PRs are recruited and that the early transcription does not result in protein production.

Longer off-intervals correspond to more cells taking Ss-OFF fate

We next used HCR to compare *ss* expression in retina progenitor cells in control vs. *ss*-snail promoter-swap backgrounds. Confocal images of HCR stains were converted into heatmaps, and active sites of transcription were quantified in regions marked by squares at 7 positions along the anterior/posterior axis (Figures 4A and S4A). We observed fewer sites of transcription in *ss*-snail promoter-swap retinas, especially posterior to the early stripe pattern (Figure 4B). Because the furrow progresses at a constant rate,[59] the observed decrease in the number of progenitor cells that actively transcribe *ss* in more posterior positions suggests they have a decreased probability of transcribing *ss* over time. In *ss*-snail, the fraction active decreases more dramatically, suggesting that *ss* transcription is more likely to turn off over time than in WT.

We next imaged *ss* transcription *in vivo* in retina progenitor cells in control and *ss*-snail L3 eye discs (Figures 4C, 4D, and S4B–S4E). Figure 4C shows frames from movies of *ss* transcription in each background, with a live-tissue DNA dye shown in magenta and MCP-GFP in green. The ability to visualize all nuclei allowed us to locate the MF and retina progenitor cells. We observed fewer sites of active transcription in the *ss*-snail line

compared with the control background (average 155 vs. 438 detections per movie), with an increase in long-duration bursts (Figure 4D left, Wilcoxon rank-sum test with continuity correction, $p = 4.785 \times 10^{-4}$).

One of the most notable differences in the remaining *ss*-transcribing cells is the long tail in the distribution of off-intervals observed for *ss-snail* (Figure 4D, bottom right). We used a Bayesian approach to test whether the data are consistent with being generated by a Poisson process. Under a Poisson process, the distribution of off-interval durations would be exponentially distributed and history-independent. We estimated the posterior distributions of the rates of turning on or off for each genotype given the data and used these rates to compute the expected distribution of durations if the Poisson model were appropriate (Figure 4D). Although the distribution of WT off-durations was generally consistent with a Poisson process, a history-independent model cannot reproduce the *ss-snail* off-interval distribution (posterior predictive *p* value: WT = 0.672; *ss-snail* = 0.0001) (see STAR Methods), suggesting that changes in some aspect of cell state during the off-period might affect the process by which cells turn back on and decrease its probability. Note that only cells that switched from off to on during our 30-min observation window are included in our data, and the tail may in fact stretch further. We then compared the 2 distributions of off-durations and found that *ss-snail* is significantly more skewed than WT ($p = 3.58 \times 10^{-2}$), suggesting a larger effect in the background in which more cells turn off.

In summary, fixed-tissue imaging uncovered a decreasing fraction of cells that actively transcribe *ss* over time (by position) in retina progenitor cells, while live imaging indicates that the type of core promoter can influence patterns of transcriptional bursting in retina progenitor cells. In a background that produces a lower Ss-ON ratio in adults, we observed fewer cells that actively transcribe *ss* and present evidence that new transcription is not history-independent. We conclude that the amount of transcriptional activity can influence the fraction of nuclei that remain active in the retina progenitor cells and therefore the final ratio of cell types produced.

Continuous transcription in progenitor cells leads to Ss-ON fate

Our results suggest that the amount and timing of *ss* transcription in retina progenitor cells may be critical for specifying Ss-ON fate in R7 PRs. Next, we tested whether driving more continuous transcription that decreases off-intervals also increases the fraction that take Ss-ON fate and express Rh4 4 days later.

We used Mirror-GAL4 to drive UAS-dCas9-VP64-p65-Rta (VPR) fusion protein in the presence of gRNAs targeted to the *ss* promoter region (Figures 5A–5C). Catalytically inactivated, non-cutting dCas9 can be fused to other types of effector proteins, in this case VPR, a potent transcriptional activator.[62] Mirror-GAL4 drives expression in the dorsal half of the eye disc from L1 to L3 in regions anterior to the MF. Expression of Mirror-GAL4 diminishes after the furrow, but to ensure temporal restriction to the early period, we included lGMR-GAL80. lGMR drives strong expression in all PRs (Figure S2B), while GAL80 blocks any residual activity of GAL4 as cells differentiate into PRs.

In this genetic background, we examined *ss* expression at L3 and Rh expression in the adult retina (Figures 5A–5C). Figure 5A shows the combined activities of endogenous *ss* transcription plus dorsal ectopic activation produced by dCas9-VPR. Compared with Figure 3E, additional sites of transcription appear across the dorsal eye disc (Figures S5A and S5B). Multiple independent sets of guide RNAs targeting the *ss* locus were tested and found to produce the same effect (Figure S5C). In the stripe region and retina progenitor cells after the furrow, we showed that *ss* transcript is not made into Ss protein. In this experiment, a high level of ectopic expression using dCas9-VPR was able to overcome this post-transcriptional block in a variable manner (Figure S5D). This additional early transcription leads to 100% dorsal Ss-ON fates as marked by R8 PR Rh expression at adult stages (Figure 5B). R8 Rhs are commonly used to report the stochastic ratio because they have been shown to reliably report R7 ss status downstream of signaling. Rh expression in the R7 layer is paradoxically less reliable because dorsal R7s coexpress Rh3 and Rh4,[64] making the ratio less apparent in images and more difficult to quantify.

At mid-pupation, Ss is expressed in all dorsal R7s (Figure 5C, top). Bristle cells (asterisk) also express Ss but are not labeled by R7+R8 marker Spalt (Sal). Normal stochastic Ss expression is observed in ventral regions where Mirror-GAL4 is not active (Figure 5C, bottom). Importantly, cell types such as outer PRs and pigment cells do not express Ss even in dorsal regions at pupal stages, indicating successful temporal restriction of ectopic activation (Figure S5E). Together, these results indicate that the continuity of transcription in the early progenitor cells controls the stochastic choice of whether to become Ss-ON.

Adding additional exogenous transcript in the early period does not affect the outcome

Our results suggest a model in which the pattern of transcription over time controls the Ss-ON ratio and where the duration and timing of off-intervals are important. An alternate model is that the total *amount* of transcription could control the ON/OFF outcome. To test whether the amount matters (as opposed to the pattern), we expressed additional *ss* mRNA in retina progenitor cells using wGMR-GAL4. The same driver was used for *in vivo* imaging in Figure 4, demonstrating activity in retina progenitor cells. When ectopic Ss is driven in the early period (together with lGMR-GAL80 to temporally limit expression), we observed no significant difference in the adult ratio (Figure S5F). This suggests that there is not a mechanism for measuring the amount of *ss* transcript present in the cell. It remains possible that the amount of transcription, rather than the amount of transcript, influences the outcome, and so we next sought an alternate way to transiently interrupt *ss* transcription.

An alternate means of introducing gaps in transcription results in Ss-OFF fate

Results from the dCas9-VPR experiment demonstrate that continuous transcription in the early period can produce 100% Ss-ON outcomes. We next asked the opposite: what happens if *ss* transcription is interrupted? With no effective dCas9-repressor fusions available in *Drosophila*, we instead examined what happens in ectopically produced R7s (Figures 5D–5F). The transcription factor Lozenge (Lz) is normally expressed in
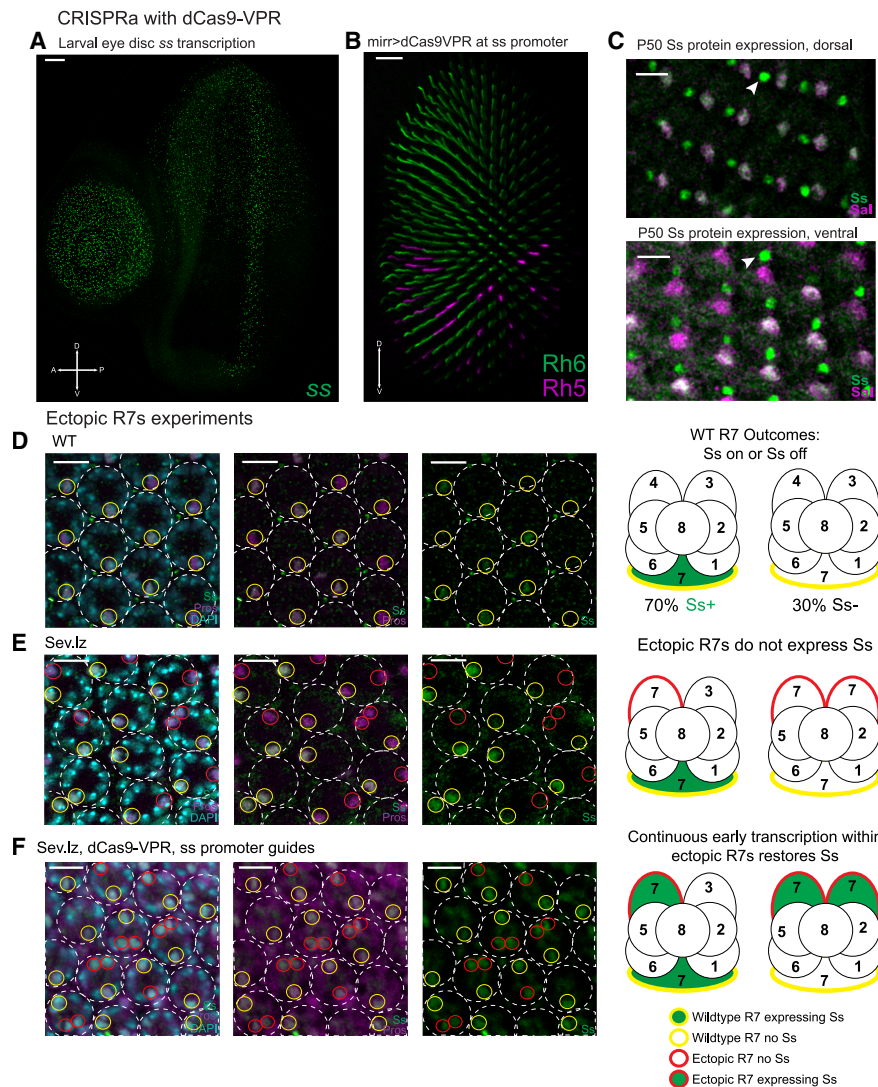
Current Biology
Article

CellPress

Figure 5. Continuity of transcription is required for Ss-ON fate

(A–C) CRISPRa: *ss* transcription is driven ectopically in the dorsal half of the eye disc using Mirror-GAL4 and UAS-dCas9-VPR in the presence of guide RNAs targeted to the *ss* locus.

lGMR-GAL80 is included to block expression in PRs as they are patterned to ensure that ectopic GAL4-based dCas9-VPR activation is temporally restricted.

(A) HCR *in situ* hybridization for *ss* introns in an L3 eye disc in this background. Scale bar, 20 μm.

(B) Adult retina Rh IHC for Rh5 and Rh6, with the dorsal retina completely converted from a stochastic cell fate to Rh6 and the ventral retina as a WT control. Scale bar, 20 μm.

(C) Mid-pupal retina with expression of Ss in R7s (marked by SalC, R7 + R8 marker, in magenta) in dorsal (top) and ventral (bottom) regions. All dorsal R7s express Ss, while in ventral R7s the pattern is stochastic. Non-R7 dorsal cell types have lost ectopic Ss expression by mid-pupation. Arrowheads mark Ss-positive, Sal-negative bristle cells. Scale bar, 10 μm.

(D–F) Transcriptional interruption: ectopic R7 PRs are produced in the R3/4 position using sev.lz, as in Mavromatakis and Tomlinson et al.[63] Ss (green), Pros (magenta, R7 marker), and DAPI (cyan). Scale bars, 10 μm.

(D) Mid-pupal WT retina showing the stochastic pattern of Ss expression in a subset of R7 PRs. Some R7s are white (co-expression of green and magenta).

(E) Mid-pupal retina in a sev.lz genetic background. Ectopic R7s are circled in red, and none express Ss.

(F) Rescue experiment in which dCas9-VPR was used to drive ectopic *ss* expression through the early period in retina progenitor cells using Mirror-GAL4, dorsal P50 retina.

See also Figure S5 and Tables S2 and S4.

R7s and is critical for their recruitment. Expressing Lz in R3/4 cells using a previously characterized *sevenless* enhancer (sev. lz) causes some R3 and R4 cells to be ectopically converted to R7s.[63] These ectopic R7s express R7 marker Prospero (Pros)

(Figure 5F). Interestingly, none of the ectopic R7s express Ss in mid-pupal retinas (236 R7s in 115 ommatidia, 121 of which were ectopic R7s; Figures 5E and S5G). Though converting R3/4 causes ommatidial rotation defects, the position of the
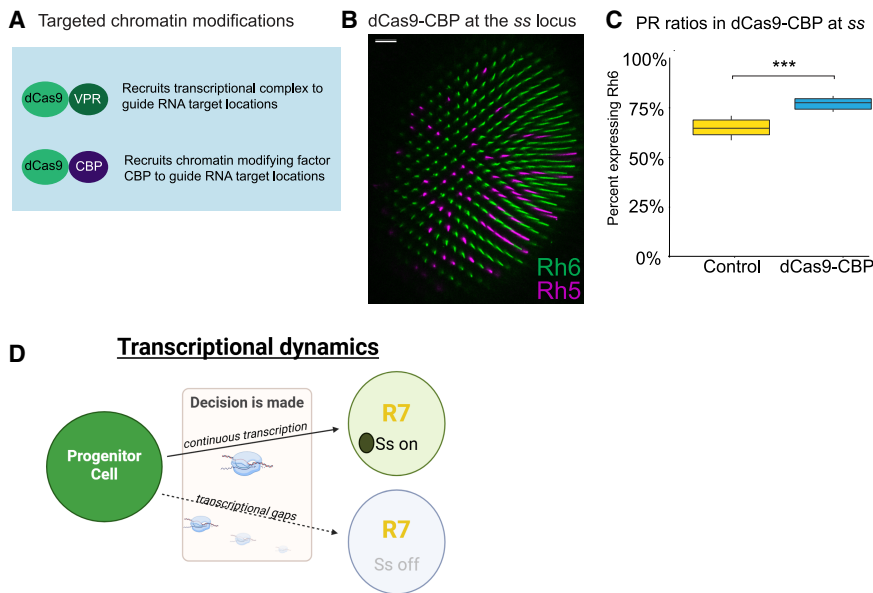
A Targeted chromatin modifications

dCas9 VPR — Recruits transcriptional complex to guide RNA target locations

dCas9 CBP — Recruits chromatin modifying factor CBP to guide RNA target locations

B dCas9-CBP at the *ss* locus

Rh6
Rh5

C PR ratios in dCas9-CBP at *ss*

***

D Transcriptional dynamics

Progenitor Cell

Decision is made
continuous transcription
transcriptional gaps

R7 Ss on

R7 Ss off

Figure 6. Targeted chromatin opening results in higher Ss-ON ratios
(A) Diagram describing the two dCas9-fusion proteins used in this study.
(B) Representative adult retina stained for Rh5 and Rh6 from the dCas9-CBP experiment, where CBP is targeted to the *ss* locus. Scale bar, 20 μm.
(C) Quantification of adult PR ratios, in which dCas9-CBP driven by wGMR-GAL4 is targeted to the *ss* promoter by guide RNAs in R7 PRs ($n = 7$; 2,559 total ommatidia), compared with controls (same genotype without guides, $n = 7$; 2,373 total ommatidia), two-tailed independent t test, $p = 0.0001$.
(D) A summary of the model that increased off-period duration and frequency leads to more cells taking Ss-OFF fate.
See also Figure S6 and Tables S2 and S4.

original R7 can be identified by staining for the R1/6 marker bar (Figure S5H). We examined sev.lz L3 eye discs and found ectopic R7s in the R3/4 position that express the R7 marker Runt but also the outer PR marker Rough (Figure S5I), indicating that ectopic R7s generated in this way pass through a period in which they are no longer progenitor cells but not yet R7s, introducing a transient gap in *ss* expression. Ectopically produced R7s fail to make a new stochastic choice of whether to express Ss, supporting the hypothesis that gaps in transcription result in Ss-OFF fate.

We then performed a rescue experiment in the sev.lz background to determine whether continuous early transcriptional activation during the transient R3/4 specification period can maintain the possibility of Ss-ON fate in ectopic R7s. As before, we used Mirror-GAL4 to drive UAS-dCas9-VPR in the dorsal half of developing sev.lz L3 retinas with gRNAs targeted to the *ss* promoter. By mid-pupation, Ss expression is restricted to normal or ectopic R7s (indicating expression is no longer dCas9-VPR-driven), and many ectopic R7s now express Ss (Figure 5F). These results indicate that removing the gap in transcription restores the possibility of Ss-ON fate.

Targeted chromatin modification
Something other than autoregulation must provide feedback to ensure that Ss becomes fully on or off, and the lack of Ss protein production in this period makes it less likely downstream transcription factors are involved. We hypothesized that chromatin state might play this role. We used dCas9-CBP to modify chromatin at the Ss locus and evaluated the resulting ommatidial ratios in the retina. Under the control of UAS/GAL4, dCas9 is fused to the acetyltransferase CBP (P300 in vertebrates).[49,65] CBP is unable to activate transcription on its own and is thought to be a pure chromatin modifier.[66] We used guide RNAs targeting the *ss* locus together with dCas9-CBP driven by wGMR-GAL4 (Figures 6A–6C).

Unlike with dCas9-VPR, expression of dCas9-CBP does not cause ectopic expression of *ss* in non-R7 cells such as outer PRs, cone cells, or pigment cells (Figure S6A), supporting the idea that CBP is not a general transcriptional activator. We observed a 10% increase in the Rh6 ratio compared with WT (Figure 6C, $p = 0.0001$). GAL4 drivers that turn on earlier and which might yield a stronger effect, such as Mirror-GAL4 or Ey3.5-GAL4, were lethal early, likely due to leaky expression in other cell types. The change in ratio indicates that chromatin state can influence the stochastic outcome, implicating a role for chromatin-based repression in cells that stop transcribing *ss* and in maintaining *ss*-OFF outcomes.

DISCUSSION

Through a combination of genome editing, live imaging of transcription, and the use of targeted dCas9 fusions, we demonstrate that future R7 subtype is determined earlier than expected and depends on the amount and timing of transcription of *ss* in retina progenitor cells. Transcription is an inherently stochastic process, and our results suggest that this variability can influence the distribution of cell types produced (summarized in Figure 6D).

Model for the production of probabilistic ratios
Studies of biological systems that produce fully divergent on or off outcomes suggest that feedback is necessary to amplify initial cell-intrinsic variability.[55,56] Our results suggest a model in which there is sufficient *ss* transcriptional activity in ~70% of retina progenitor cells to maintain an ON state until R7 recruitment, while ~30% have gaps in transcription long enough to result in the locus becoming inactive. We suggest that chromatin state could be modified during gaps in active transcription to reduce the probability of new transcription. This could provide a means of negative feedback to allow these cells to achieve a fully Ss-OFF state. This model does not directly explain the observed reliability of the stochastic ratio from animal to animal, which would be interesting to investigate further.

Current Biology
Article

⌘ CellPress

Patterns over time

It is important to note that different patterns of transcriptional bursting could lead to production of the same amount of protein when averaged over time. Two large bursts could produce the same total number of mRNAs as many small bursts, which in many cases is unlikely to have functional consequences. Because Ss protein is absent and does not play a role when the decision is made during R7 specification, we conclude that the amount or timing of transcription itself controls the outcome. Whether the process of transcription acts to keep the locus accessible or whether the mRNA plays a more active role remains an open question, though *ss* overexpression in the early period (Figure S5F) did not change the stochastic outcome. It would be interesting to determine whether similar mechanisms influence other cell fate decisions.

Other developmental contexts

It is possible that the continuity of transcription plays a role in other stochastic cell fate specification contexts. While stochastic and deterministic patterning are sometimes described as fundamentally different mechanisms of cell fate specification, in some contexts, such as at the boundaries of gene expression domains where cells make a cell-by-cell decision to turn a gene fully ON or OFF, there may be similarities. In some cases, perhaps similar mechanisms play a role as in stochastic patterning in the fly retina. Such a scenario could potentially help explain how stochastic patterning originally evolved.

In summary, we have presented evidence that patterns of transcriptional bursting over time influence the stochastic ratio of cell fates produced in the *Drosophila* retina. Modifying the patterns of transcriptional bursting or changing chromatin accessibility changes this ratio, suggesting that a corresponding change in upstream transcription factor expression is not required and implicating chromatin state as the negative force acting in the absence of continuous transcription. These results suggest that continuous transcriptional activation is sufficient to produce ON outcomes and that chromatin modification occurs only during dynamic and variable gaps in active transcription. We suggest that the frequency and duration of these gaps therefore control the OFF outcome and the ratio of cells that ultimately take divergent fates.

RESOURCE AVAILABILITY

Lead contact

Requests for further information and resources should be directed to lead contact, Michael Perry (mwperry@ucsd.edu).

Materials availability

All fly lines generated in this study are available from the lead contact without restriction. Correspondence and requests for materials should be addressed to mwperry@ucsd.edu.

Data and code availability

- All data reported in this paper will be shared by the lead contact upon request.
- All code generated for this study can be found at https://doi.org/10.5281/zenodo.15368487 and is publicly available as of the date of publication. https://github.com/Yzhao4707/Ss_Dynamics.
- Any additional information required to reanalyze the data reported in this work paper is available from the lead contact upon request.

DECLARATION OF INTERESTS

The authors declare no competing interests.

STAR★METHODS

Detailed methods are provided in the online version of this paper and include the following:

- KEY RESOURCES TABLE
- EXPERIMENTAL MODEL AND STUDY PARTICIPANT DETAILS
  - *Drosophila* Rearing
  - Transient ss overexpression
- METHOD DETAILS
  - Nomenclature
  - Confocal Imaging
  - Immunohistochemistry
  - CRISPR Guide Design
  - Cloning and Generation of Transgenic fly stocks
  - FlpD5-T2A-ss CRISPR KI
  - Ss intronic MS2 Repeats
  - R7 reporter pm181-mCherry
  - *In Situ* Hybridization
  - Live Imaging
  - Controlling for MCP-GFP aggregation
- QUANTIFICATION AND STATISTICAL ANALYSIS
  - Quantification and statistics of IHC tissue
  - Analysis of HCR *in situ* hybridization stains
  - Analysis of live MS2 movies
  - Statistical tests of ON and OFF period distributions

SUPPLEMENTAL INFORMATION

Supplemental information can be found online at https://doi.org/10.1016/j.cub.2025.05.037.

REFERENCES

1. Garcia, H.G., Tikhonov, M., Lin, A., and Gregor, T. (2013). Quantitative imaging of transcription in living Drosophila embryos links polymerase activity to patterning. Curr. Biol. *23*, 2140–2145. https://doi.org/10.1016/j.cub.2013.08.054.

2. Bothma, J.P., Garcia, H.G., Esposito, E., Schlissel, G., Gregor, T., and Levine, M. (2014). Dynamic regulation of *eve* stripe 2 expression reveals transcriptional bursts in living *Drosophila* embryos. Proc. Natl. Acad. Sci. USA *111*, 10598–10603. https://doi.org/10.1073/pnas.1410022111.

3. Zhao, J., Perkins, M.L., Norstad, M., and Garcia, H.G. (2023). A bistable autoregulatory module in the developing embryo commits cells to binary expression fates. Curr. Biol. *33*, 2851–2864.e11. https://doi.org/10.1016/j.cub.2023.06.060.

4. Birnie, A., Plat, A., Korkmaz, C., and Bothma, J.P. (2023). Precisely timed regulation of enhancer activity defines the binary expression pattern of Fushi tarazu in the Drosophila embryo. Curr. Biol. *33*, 2839–2850.e7. https://doi.org/10.1016/j.cub.2023.04.005.

5. Lim, B., Fukaya, T., Heist, T., and Levine, M. (2018). Temporal dynamics of pair-rule stripes in living *Drosophila* embryos. Proc. Natl. Acad. Sci. USA *115*, 8376–8381. https://doi.org/10.1073/pnas.1810430115.

6. Lin, S., and Lim, B. (2024). Multifaceted effects on *even-skipped* transcriptional dynamics upon *Krüppel* dosage changes. Development *151*, dev202132. https://doi.org/10.1242/dev.202132.

7. Lim, B. (2018). Imaging transcriptional dynamics. Curr. Opin. Biotechnol. *52*, 49–55. https://doi.org/10.1016/j.copbio.2018.02.008.

8. Perry, M.W., Boettiger, A.N., Bothma, J.P., and Levine, M. (2010). Shadow Enhancers Foster Robustness of Drosophila Gastrulation. Curr. Biol. *20*, 1562–1567. https://doi.org/10.1016/j.cub.2010.07.043.

9. Lagha, M., Bothma, J.P., Esposito, E., Ng, S., Stefanik, L., Tsui, C., Johnston, J., Chen, K., Gilmour, D.S., Zeitlinger, J., et al. (2013). Paused Pol II coordinates tissue morphogenesis in the Drosophila embryo. Cell *153*, 976–987. https://doi.org/10.1016/j.cell.2013.04.045.

10. Shao, W., and Zeitlinger, J. (2017). Paused RNA polymerase II inhibits new transcriptional initiation. Nat. Genet. *49*, 1045–1051. https://doi.org/10.1038/ng.3867.

11. Tantale, K., Mueller, F., Kozulic-Pirher, A., Lesne, A., Victor, J.-M., Robert, M.-C., Capozi, S., Chouaib, R., Bäcker, V., Mateos-Langerak, J., et al. (2016). A single-molecule view of transcription reveals convoys of RNA polymerases and multi-scale bursting. Nat. Commun. *7*, 12248. https://doi.org/10.1038/ncomms12248.

12. Lucas, T., Ferraro, T., Roelens, B., De Las Heras Chanes, J., Walczak, A.M., Coppey, M., and Dostatni, N. (2013). Live Imaging of Bicoid-Dependent Transcription in Drosophila Embryos. Curr. Biol. *23*, 2135–2139. https://doi.org/10.1016/j.cub.2013.08.053.

13. Levo, M., Raimundo, J., Bing, X.Y., Sisco, Z., Batut, P.J., Ryabichko, S., Gregor, T., and Levine, M.S. (2022). Transcriptional coupling of distant regulatory genes in living embryos. Nature *605*, 754–760. https://doi.org/10.1038/s41586-022-04680-7.

14. Lammers, N.C., Kim, Y.J., Zhao, J., and Garcia, H.G. (2020). A matter of time: Using dynamics and theory to uncover mechanisms of transcriptional bursting. Curr. Opin. Cell Biol. *67*, 147–157. https://doi.org/10.1016/j.ceb.2020.08.001.

15. Park, J., Estrada, J., Johnson, G., Vincent, B.J., Ricci-Tam, C., Bragdon, M.D., Shulgina, Y., Cha, A., Wunderlich, Z., Gunawardena, J., et al. (2019). Dissecting the sharp response of a canonical developmental enhancer reveals multiple sources of cooperativity. eLife *8*, e41266. https://doi.org/10.7554/eLife.41266.

16. Eck, E., Liu, J., Kazemzadeh-Atoufi, M., Ghoreishi, S., Blythe, S.A., and Garcia, H.G. (2020). Quantitative dissection of transcription in development yields evidence for transcription-factor-driven chromatin accessibility. eLife *9*, e56429. https://doi.org/10.7554/eLife.56429.

17. Batut, P.J., Bing, X.Y., Sisco, Z., Raimundo, J., Levo, M., and Levine, M.S. (2022). Genome organization controls transcriptional dynamics during development. Science *375*, 566–570. https://doi.org/10.1126/science.abi7178.

18. Perry, M.W., Boettiger, A.N., and Levine, M. (2011). Multiple enhancers ensure precision of gap gene-expression patterns in the *Drosophila* embryo. Proc. Natl. Acad. Sci. USA *108*, 13570–13575. https://doi.org/10.1073/pnas.1109873108.

19. Bothma, J.P., Garcia, H.G., Ng, S., Perry, M.W., Gregor, T., and Levine, M. (2015). Enhancer additivity and non-additivity are determined by enhancer strength in the Drosophila embryo. eLife *4*, e07956. https://doi.org/10.7554/eLife.07956.

20. Frankel, N., Davis, G.K., Vargas, D., Wang, S., Payre, F., and Stern, D.L. (2010). Phenotypic robustness conferred by apparently redundant transcriptional enhancers. Nature *466*, 490–493. https://doi.org/10.1038/nature09158.

21. Bothma, J.P., Norstad, M.R., Alamos, S., and Garcia, H.G. (2018). LlamaTags: A Versatile Tool to Image Transcription Factor Dynamics in Live Embryos. Cell *173*, 1810–1822.e16. https://doi.org/10.1016/j.cell.2018.03.069.

22. Little, S.C., Tikhonov, M., and Gregor, T. (2013). Precise Developmental Gene Expression Arises from Globally Stochastic Transcriptional Activity. Cell *154*, 789–800. https://doi.org/10.1016/j.cell.2013.07.025.

23. Huang, A., Amourda, C., Zhang, S., Tolwinski, N.S., and Saunders, T.E. (2017). Decoding temporal interpretation of the morphogen Bicoid in the early Drosophila embryo. eLife *6*, e26258. https://doi.org/10.7554/eLife.26258.

24. Elowitz, M.B., Levine, A.J., Siggia, E.D., and Swain, P.S. (2002). Stochastic Gene Expression in a Single Cell. Science *297*, 1183–1186. https://doi.org/10.1126/science.1070919.

25. Thattai, M., and van Oudenaarden, A. (2004). Stochastic gene expression in fluctuating environments. Genetics *167*, 523–530. https://doi.org/10.1534/genetics.167.1.523.

26. Losick, R., and Desplan, C. (2008). Stochasticity and Cell Fate. Science *320*, 65–68. https://doi.org/10.1126/science.1147888.

27. Gefen, O., and Balaban, N.Q. (2009). The importance of being persistent: heterogeneity of bacterial populations under antibiotic stress. FEMS Microbiol. Rev. *33*, 704–717. https://doi.org/10.1111/j.1574-6976.2008.00156.x.

28. Zechner, C., Nerli, E., and Norden, C. (2020). Stochasticity and determinism in cell fate decisions. Development *147*, dev181495. https://doi.org/10.1242/dev.181495.

29. Serizawa, S., Miyamichi, K., Nakatani, H., Suzuki, M., Saito, M., Yoshihara, Y., and Sakano, H. (2003). Negative feedback regulation ensures the one receptor-one olfactory neuron rule in mouse. Science *302*, 2088–2094. https://doi.org/10.1126/science.1089122.

30. Ng, K.K., Yui, M.A., Mehta, A., Siu, S., Irwin, B., Pease, S., Hirose, S., Elowitz, M.B., Rothenberg, E.V., and Kueh, H.Y. (2018). A stochastic epigenetic switch controls the dynamics of T-cell lineage commitment. eLife *7*, e37851. https://doi.org/10.7554/eLife.37851.

31. Johnston, R.J., and Desplan, C. (2010). Stochastic mechanisms of cell fate specification that yield random or robust outcomes. Annu. Rev. Cell Dev. Biol. *26*, 689–719. https://doi.org/10.1146/annurev-cellbio-100109-104113.

32. Bell, M.L., Earl, J.B., and Britt, S.G. (2007). Two types of *Drosophila* R7 photoreceptor cells are arranged randomly: A model for stochastic cell-fate determination. J. Comp. Neurol. *502*, 75–85. https://doi.org/10.1002/cne.21298.

33. Thanawala, S.U., Rister, J., Goldberg, G.W., Zuskov, A., Olesnicky, E.C., Flowers, J.M., Jukam, D., Purugganan, M.D., Gavis, E.R., Desplan, C., et al. (2013). Regional Modulation of a Stochastically Expressed Factor Determines Photoreceptor Subtypes in the Drosophila Retina. Dev. Cell *25*, 93–105. https://doi.org/10.1016/j.devcel.2013.02.016.

34. Ordway, A.J., Helt, R.N., and Johnston, R.J. (2024). Transcriptional priming and chromatin regulation during stochastic cell fate specification.

Philos. Trans. R. Soc. Lond. B Biol. Sci. *379*, 20230046. https://doi.org/10.1098/rstb.2023.0046.

35. Wernet, M.F., Mazzoni, E.O., Çelik, A., Duncan, D.M., Duncan, I., and Desplan, C. (2006). Stochastic spineless expression creates the retinal mosaic for colour vision. Nature *440*, 174–180. https://doi.org/10.1038/nature04615.

36. Mikeladze-Dvali, T., Wernet, M.F., Pistillo, D., Mazzoni, E.O., Teleman, A.A., Chen, Y.-W., Cohen, S., and Desplan, C. (2005). The growth regulators warts/lats and melted interact in a bistable loop to specify opposite fates in Drosophila R8 photoreceptors. Cell *122*, 775–787. https://doi.org/10.1016/j.cell.2005.07.026.

37. Jukam, D., and Desplan, C. (2011). Binary regulation of Hippo pathway by Merlin/NF2, Kibra, Lgl, and Melted specifies and maintains postmitotic neuronal fate. Dev. Cell *21*, 874–887. https://doi.org/10.1016/j.devcel.2011.10.004.

38. Jukam, D., Xie, B., Rister, J., Terrell, D., Charlton-Perkins, M., Pistillo, D., Gebelein, B., Desplan, C., and Cook, T. (2013). Opposite feedbacks in the Hippo pathway for growth control and neural fate. Science *342*, 1238016. https://doi.org/10.1126/science.1238016.

39. Johnston, R.J., and Desplan, C. (2014). Interchromosomal communication coordinates intrinsically stochastic expression between alleles. Science *343*, 661–665. https://doi.org/10.1126/science.1243039.

40. Wells, B.S., Pistillo, D., Barnhart, E., and Desplan, C. (2017). Parallel Activin and BMP signaling coordinates R7/R8 photoreceptor subtype pairing in the stochastic Drosophila retina. eLife *6*, e25301. https://doi.org/10.7554/eLife.25301.

41. Yan, J., Anderson, C., Viets, K., Tran, S., Goldberg, G., Small, S., and Johnston, R.J. (2017). Regulatory logic driving stable levels of *defective proventriculus* expression during terminal photoreceptor specification in flies. Development *144*, 844–855. https://doi.org/10.1242/dev.144030.

42. Rister, J., Razzaq, A., Boodram, P., Desai, N., Tsanis, C., Chen, H., Jukam, D., and Desplan, C. (2015). Single-base pair differences in a shared motif determine differential Rhodopsin expression. Science *350*, 1258–1261. https://doi.org/10.1126/science.aab3417.

43. Poupault, C., Choi, D., Lam-Kamath, K., Dewett, D., Razzaq, A., Bunker, J., Perry, A., Cho, I., and Rister, J. (2021). A combinatorial cis-regulatory logic restricts color-sensing Rhodopsins to specific photoreceptor subsets in Drosophila. PLoS Genet. *17*, e1009613. https://doi.org/10.1371/journal.pgen.1009613.

44. Wernet, M.F., Labhart, T., Baumann, F., Mazzoni, E.O., Pichaud, F., and Desplan, C. (2003). Homothorax switches function of Drosophila photoreceptors from color to polarized light sensors. Cell *115*, 267–279. https://doi.org/10.1016/s0092-8674(03)00848-1.

45. Voortman, L., Anderson, C., Urban, E., Yuan, L., Tran, S., Neuhaus-Follini, A., Derrick, J., Gregor, T., and Johnston, R.J. (2022). Temporally dynamic antagonism between transcription and chromatin compaction controls stochastic photoreceptor specification in flies. Dev. Cell *57*, 1817–1832. e5. https://doi.org/10.1016/j.devcel.2022.06.016.

46. Bertrand, E., Chartrand, P., Schaefer, M., Shenoy, S.M., Singer, R.H., and Long, R.M. (1998). Localization of ASH1 mRNA Particles in Living Yeast. Mol. Cell *2*, 437–445. https://doi.org/10.1016/s1097-2765(00)80143-4.

47. Yamada, S., Whitney, P.H., Huang, S.-K., Eck, E.C., Garcia, H.G., and Rushlow, C.A. (2019). The Drosophila Pioneer Factor Zelda Modulates the Nuclear Microenvironment of a Dorsal Target Enhancer to Potentiate Transcriptional Output. Curr. Biol. *29*, 1387–1393.e5. https://doi.org/10.1016/j.cub.2019.03.019.

48. Ewen-Campen, B., Yang-Zhou, D., Fernandes, V.R., González, D.P., Liu, L.-P., Tao, R., Ren, X., Sun, J., Hu, Y., Zirin, J., et al. (2017). Optimized strategy for in vivo Cas9-activation in *Drosophila*. Proc. Natl. Acad. Sci. USA *114*, 9409–9414. https://doi.org/10.1073/pnas.1707635114.

49. Sajwan, S., and Mannervik, M. (2019). Gene activation by dCas9-CBP and the SAM system differ in target preference. Sci. Rep. *9*, 18104. https://doi.org/10.1038/s41598-019-54179-x.

50. Leyes Porello, E.A., Trudeau, R.T., and Lim, B. (2023). Transcriptional bursting: stochasticity in deterministic development. Development *150*, dev201546. https://doi.org/10.1242/dev.201546.

51. Jinek, M., Chylinski, K., Fonfara, I., Hauer, M., Doudna, J.A., and Charpentier, E. (2012). A programmable dual-RNA-guided DNA endonuclease in adaptive bacterial immunity. Science *337*, 816–821. https://doi.org/10.1126/science.1225829.

52. Lee, C.H., Herman, T., Clandinin, T.R., Lee, R., and Zipursky, S.L. (2001). N-Cadherin Regulates Target Specificity in the Drosophila Visual System. Neuron *30*, 437–450. https://doi.org/10.1016/s0896-6273(01)00291-4.

53. Rintelen, F., Hafen, E., and Nairz, K. (2003). The *Drosophila* dual-specificity ERK phosphatase DMKP3 cooperates with the ERK tyrosine phosphatase PTP-ER. Development *130*, 3479–3490. https://doi.org/10.1242/dev.00568.

54. Carrillo, R.A., Özkan, E., Menon, K.P., Nagarkar-Jaiswal, S., Lee, P.-T., Jeon, M., Birnbaum, M.E., Bellen, H.J., Garcia, K.C., and Zinn, K. (2015). Control of synaptic connectivity by a network of Drosophila IgSF cell surface proteins. Cell *163*, 1770–1782. https://doi.org/10.1016/j.cell.2015.11.022.

55. Süel, G.M., Garcia-Ojalvo, J., Liberman, L.M., and Elowitz, M.B. (2006). An excitable gene regulatory circuit induces transient cellular differentiation. Nature *440*, 545–550. https://doi.org/10.1038/nature04588.

56. Mugler, A., Kittisopikul, M., Hayden, L., Liu, J., Wiggins, C.H., Süel, G.M., and Walczak, A.M. (2016). Noise Expands the Response Range of the Bacillus subtilis Competence Circuit. PLoS Comput. Biol. *12*, e1004793. https://doi.org/10.1371/journal.pcbi.1004793.

57. Choi, H.M.T., Schwarzkopf, M., Fornace, M.E., Acharya, A., Artavanis, G., Stegmaier, J., Cunha, A., and Pierce, N.A. (2018). Third-generation in situ hybridization chain reaction: multiplexed, quantitative, sensitive, versatile, robust. Development *145*, dev165753. https://doi.org/10.1242/dev.165753.

58. Duncan, D.M., Burgess, E.A., and Duncan, I. (1998). Control of distal antennal identity and tarsal development in Drosophila by spineless-aristapedia, a homolog of the mammalian dioxin receptor. Genes Dev. *12*, 1290–1303. https://doi.org/10.1101/gad.12.9.1290.

59. Roignant, J.-Y., and Treisman, J.E. (2009). Pattern formation in the Drosophila eye disc. Int. J. Dev. Biol. *53*, 795–804. https://doi.org/10.1387/ijdb.072483jr.

60. Ready, D.F. (1989). A multifaceted approach to neural development. Trends Neurosci. *12*, 102–110. https://doi.org/10.1016/0166-2236(89)90166-5.

61. Evans, C.J., Olson, J.M., Ngo, K.T., Kim, E., Lee, N.E., Kuoy, E., Patananan, A.N., Sitz, D., Tran, P., Do, M.-T., et al. (2009). G-TRACE: rapid Gal4-based cell lineage analysis in Drosophila. Nat. Methods *6*, 603–605. https://doi.org/10.1038/nmeth.1356.

62. Chavez, A., Scheiman, J., Vora, S., Pruitt, B.W., Tuttle, M., P R Iyer, E., Lin, S., Kiani, S., Guzman, C.D., Wiegand, D.J., et al. (2015). Highly efficient Cas9-mediated transcriptional programming. Nat. Methods *12*, 326–328. https://doi.org/10.1038/nmeth.3312.

63. Mavromatakis, Y.E., and Tomlinson, A. (2013). Switching cell fates in the developing Drosophila eye. Development *140*, 4353–4361. https://doi.org/10.1242/dev.096925.

64. Mazzoni, E.O., Celik, A., Wernet, M.F., Vasiliauskas, D., Johnston, R.J., Cook, T.A., Pichaud, F., and Desplan, C. (2008). Iroquois Complex Genes Induce Co-Expression of rhodopsins in Drosophila. PLoS Biol. *6*, e97. https://doi.org/10.1371/journal.pbio.0060097.

65. Hilton, I.B., D'Ippolito, A.M., Vockley, C.M., Thakore, P.I., Crawford, G.E., Reddy, T.E., and Gersbach, C.A. (2015). Epigenome editing by a CRISPR-Cas9-based acetyltransferase activates genes from promoters and enhancers. Nat. Biotechnol. *33*, 510–517. https://doi.org/10.1038/nbt.3199.

66. Holmqvist, P.-H., and Mannervik, M. (2013). Genomic occupancy of the transcriptional co-activators p300 and CBP. Transcription *4*, 18–23. https://doi.org/10.4161/trns.22601.

67. Schindelin, J., Arganda-Carreras, I., Frise, E., Kaynig, V., Longair, M., Pietzsch, T., Preibisch, S., Rueden, C., Saalfeld, S., Schmid, B., et al. (2012). Fiji: an open-source platform for biological-image analysis. Nat. Methods 9, 676–682. https://doi.org/10.1038/nmeth.2019.

68. Rebeiz, M., and Posakony, J.W. (2004). GenePalette: a universal software tool for genome sequence visualization and analysis. Dev. Biol. 271, 431–438. https://doi.org/10.1016/j.ydbio.2004.04.011.

69. Labun, K., Montague, T.G., Krause, M., Torres Cleuren, Y.N., Tjeldnes, H., and Valen, E. (2019). CHOPCHOP v3: expanding the CRISPR web toolbox beyond genome editing. Nucleic Acids Res. 47, W171–W174. https://doi.org/10.1093/nar/gkz365.

70. Concordet, J.-P., and Haeussler, M. (2018). CRISPOR: intuitive guide selection for CRISPR/Cas9 genome editing experiments and screens. Nucleic Acids Res. 46, W242–W245. https://doi.org/10.1093/nar/gky354.

71. Berg, S., Kutra, D., Kroeger, T., Straehle, C.N., Kausler, B.X., Haubold, C., Schiegg, M., Ales, J., Beier, T., Rudy, M., et al. (2019). ilastik: interactive machine learning for (bio)image analysis. Nat. Methods 16, 1226–1232. https://doi.org/10.1038/s41592-019-0582-9.

72. Morrison, C.M., and Halder, G. (2010). Characterization of a dorsal-eye Gal4 Line in *Drosophila*. Genesis 48, 3–7. https://doi.org/10.1002/dvg.20571.

73. Wernet, M.F., and Desplan, C. (2014). Homothorax and Extradenticle alter the transcription factor network in *Drosophila* ommatidia at the dorsal rim of the retina. Development 141, 918–928. https://doi.org/10.1242/dev.103127.

74. Gallagher, K.D., Mani, M., and Carthew, R.W. (2022). Emergence of a geometric pattern of cell fates from tissue-scale mechanics in the Drosophila eye. eLife 11, e72806. https://doi.org/10.7554/eLife.72806.

STAR★METHODS

KEY RESOURCES TABLE

REAGENT or RESOURCE	SOURCE	IDENTIFIER
Antibodies		
Guinea Pig Polyclonal Anti-Spineless (1:400)	Claude Desplan (New York University)	N/A
Mouse Monoclonal Anti-Rh3 (1:100)	Steven Britt (University of Texas at Austin Dell Medical School)	N/A
Guinea Pig Polyclonal Anti-Rh4 (1:500)	Claude Desplan (New York University)	N/A
Mouse Monoclonal Anti-Rh5 (1:100)	Steven Britt (University of Texas at Austin Dell Medical School)	N/A
Rabbit Polyclonal Anti-Rh6 (1:2000)	Claude Desplan (New York University)	N/A
Rabbit Polyclonal Anti-SalC (1:400)	Claude Desplan (New York University)	N/A
Mouse Monoclonal Anti-Prospero (1:50)	Developmental Studies Hybridoma Bank	Cat# Prospero (MR1A); RRID: AB_528440
Sheep Polyclonal Anti-GFP (1:500)	Bio-Rad	Cat# 4745-1051; RRID: AB_619712
Rabbit Polyclonal Anti-RFP (1:500)	Invitrogen	Cat# R10367
Donkey Anti Sheep IgG A488	ThermoFisher Scientific	Cat# A-11015; RRID:AB_2534082
Donkey Anti Rabbit IgG A488	ThermoFisher Scientific	Cat# A-21206; RRID: AB_2535792
Donkey Anti-Mouse IgG A555	ThermoFisher Scientific	Cat# A-31570; RRID: AB_2536180
Donkey Anti-Guinea Pig IgG A647	Jackson ImmunoResearch	Cat# 706-605-148; RRID: AB_2340476
Chemicals, peptides, and recombinant proteins		
16% Paraformaldehyde	Electron Microscopy Sciences	Cat# 15710
SlowFade Gold Antifade Mountant	Invitrogen	Cat# S36936
SiR-DNA kit	Spirochrome	Cat# SC007
Deposited data		
Repository for code used in data analysis for Figure 4D	This paper	https://doi.org/10.5281/zenodo.15368487
Experimental models: Organisms/strains		
D. melanogaster: PM181GAL4	Rintelen et al.[53]	FBal0124005
D. melanogaster: Gal80ts	Bloomington Drosophila Research Center	Cat# 7108
D. melanogaster: PM181mCherry	This paper	N/A
D. melanogaster: UAS-GFPnls	Bloomington Drosophila Research Center	Cat# 4775
D. melanogaster: sp/CyO; ss-24xMS2	This paper	N/A
D. melanogaster: Ss promoter guides #1	This paper	N/A
D. melanogaster: dCas9VPR	Bloomington Drosophila Research Center	Cat# 67051
D. melanogaster: MirrorGal4	Morrison et al.[67]	FBti0128097
D. melanogaster: UAS-MCP-GFP	This paper	N/A
D. melanogaster: wGMR-GAL4	N/A	N/A
D. melanogaster: ss-sna-24xMS2	This paper	N/A
D. melanogaster: UAS-Ss	Duncan et al.[58]	FBal0090105
D. melanogaster: Ss-flp	This paper	N/A
D. melanogaster: ubiFRT-stop-Stinger	Evans et al.[61]	N/A
D. melanogaster: lGMR-GAL80	Mathias Wernet (Freie Universitaet Berlin)	N/A
D. melanogaster: Sev.Lz	Andrew Tomlinson (Columbia University)	N/A
D. melanogaster: UAS-dCas9-CBP	Mattias Manervik (Stockholm University)	N/A
D. melanogaster: UAS-flp	Mathias Wernet (Freie Universitaet Berlin)	N/A
D. melanogaster: FRT82b, gmrhid	Mathias Wernet (Freie Universitaet Berlin)	N/A
D. melanogaster: FRT82b	Mathias Wernet (Freie Universitaet Berlin)	N/A
D. melanogaster: SsDel115.7	Mathias Wernet (Freie Universitaet Berlin)	N/A

(Continued on next page)

Continued

REAGENT or RESOURCE	SOURCE	IDENTIFIER
D. melanogaster: lGMR-GAL4	Claude Desplan (NYU)	N/A
D. melanogaster: Hsflp	Bloomington Drosophila Research Center	Cat#1929
D. melanogaster: Ss promoter guides #2	This paper	N/A
Full genotypes for every main figure reported in Table S2	This paper	N/A
Full genotypes for every supplemental figure reported in Table S3	This paper	N/A
Oligonucleotides		
Guide RNA sequences reported in Table S4	This paper	N/A
Primers for promoter swap, see Table S5	This paper	N/A
HCR probe sets reported in Table S7	This paper	N/A
Recombinant DNA		
Plasmids reported in Table S6	This paper	N/A
Software and algorithms		
Fiji (ImageJ)	https://fiji.sc	RRID: SCR_002285
R (v4.4.3)	https://cran.r-project.org/	RRID: SCR_001905
Adobe Illustrator 2024	https://www.adobe.com/uk/products/illustrator.html	RRID: SCR_010279
Microsoft Word	https://www.microsoft.com/en-gb/	N/A
Ilastik	Berg et al.[68]	RRID: SCR_015246
Biorender	https://www.biorender.com	RRID: SCR_018361
GenePalette	Rebeiz and Posakony 77	N/A
Other		
#55 Forceps	Dumostar	Cat# 11295-51

EXPERIMENTAL MODEL AND STUDY PARTICIPANT DETAILS

Drosophila Rearing
Drosophila stocks were raised at 22°C or 25°C and fed on standard cornmeal. Heat induction via GAL80ts inactivation was performed at 29°C. The specific genotypes used in the paper are listed in Table S2. Animals of both sexes were used.

Transient ss overexpression
For ectopic Ss cDNA expression, crosses were raised at 18°C until the period of ectopic activation, when they were shifted to 29°C for a period of 12 hours, then moved back to 18°C until dissection at adult stages.

METHOD DETAILS

Nomenclature
We use "Ss-ON" and "Ss-OFF" to indicate cell fate for the two R7 PR subtypes. Ss-ON is different from Ss-positive or Ss+: Ss-ON indicates fate while Ss+ indicates current state. This is important in that Ss-ON cells do not continually transcribe Ss, and so a cell that has taken the Ss-ON fate may not always be Ss+ in fixed tissue snapshots (e.g. via HCR for *ss* introns) or in single frames of movies. At adult stages, Rh4 expression is a clear indicator of Ss-ON fate, while Rh3 expression indicates Ss-OFF fate. Rhs are not expressed until very late pupal stages and cannot be used as markers until ~four days after the initial Ss-ON/OFF decision was made. At L3 in differentiated R7s we used movies to watch expression over time and identified Ss-ON vs. Ss-OFF cells, but did not have a fixed-tissue way to identify Ss-ON vs. Ss-OFF. In some cases, we quantified the fraction of Ss+ R7s in two genotypes to identify differences, but this does not conclusively identify all Ss-ON R7s. At pupal stages we used Dpr11 as a marker of Ss-ON fate, as Dpr11 turns on earlier than Rh4 in Ss-ON R7s, and turns on only in R7s that express Ss.

Confocal Imaging
Confocal images were acquired using Leica SP8 and Zeiss 700 confocal microscopes and processed using ImageJ/FIJI and Photoshop. Tissues were imaged with a 20x air or a 40x oil objective. Adult retinas were imaged at 1.5 uM intervals. Maximum intensity projections of confocal stacks are used in figures.

Current Biology
Article

🔗 **CellPress**

Immunohistochemistry

Adult, pupal, and larval retinas were freshly dissected in PBS and fixed with 4% PFA for 12-15 minutes at room temperature. The tissue was washed with PBST (0.2% Triton 100) for 5 minutes 2-3 times and then 15 minutes 2-3 times. Tissue was then blocked with a 5% NGS solution in PBST for 30 minutes at room temperature and stained with primary antibodies in a 5% NGS-PBST solution overnight. Primary antibodies were diluted at different working concentrations (see Table S3). The tissue was washed with 0.2% PBST 3 times for 5 minutes and 3 times for 20 minutes, blocked for a further 30 minutes and then stained with secondary antibodies (1:500 concentration, Invitrogen or Jackson Immuno) at room temperature for 2 hours. The tissue was washed, stained with DAPI, and mounted on microscope slides with size #1.5 coverslips using ProLong gold antifade media. Slides were sealed with clear nail polish and stored in the dark at 4°C until imaging.

CRISPR Guide Design

Online gRNA design tools ChopChop[69] and CRISPOR[70] were used to choose candidate gRNAs (19bp) for *ss* flip, dCas9, and pro-moter-swap experiments. The primers containing gRNAs were cloned into pCFD5.[71] The final plasmids were sequence-verified via Sanger or NGS sequencing. CRISPR KI repair templates were designed by selecting 1-1.5kb long homology arms flanking the site of insertion/modification. For repair templates, PBlueScript was used as backbone for ss-flp, pGEM-Teasy was used as backbone for ss-sna. *Drosophila* embryos were collected and injected by Bestgene, Inc. with repair template, Cas9, and PCFD5-gRNA plasmid. Individual G0s were crossed, balanced, and PCR screened to establish stable lines. All gRNAs used are listed in Table S4.

Cloning and Generation of Transgenic fly stocks

Ss Promoter Swap via CRISPR homology directed repair. We designed repair template plasmids to replace the core promoter of *spineless* with *snail* using CRISPR-driven homology directed repair (HDR). This modification was made using the same starting chromosome III and crossed into the same genetic background so that the only difference between *ss-snail* and WT is at the core pro-moter of the *ss* locus. The specific swapped sequences are listed in Table S1. Pooled F1 siblings (~15 from each G0 x QBs cross) were screen by PCR to identify positive parents; in these cases, surviving siblings were crossed to balancers to establish lines, which were again screened by PCR to identify successful editing events.

FlpD5-T2A-ss CRISPR KI

FlpD5-T2A was inserted at the 5' end of *ss* locus using CRISPR-driven HDR. The repair template was annealed into an empty pBlue-Script plasmid through traditional restriction enzyme cloning. The transformants were crossed with BDSC #32251 to generate FlpD5-T2A-ss/Ubi-p633E- (FRT.STOP)StingerGFP. Flp-D5 sequence used: atgccacaatttgatatattatgtaaaacaccacctaaggtgcttgttcgt cagtttgtggaaaggtttgaaagaccttcaggtgagaaaatagcattatgtgctgctgaactaacctatttatgttggatgattacacataacggaacagcaatcaagagagccacat tcatgagctataatactatcataagcaattcgctgagtttcgatattgtcaataaatcactccagtttaaatacaagacgcaaaaagcaacaattctggaagcctcattaaagaaattg attcctgcttgggaatttacaattattccttactatggacaaaaacatcaatctgatatcactgatattgtaagtagtttgcaattacagttcgaatcatcggaagaagcagataagggaa atagccacagtaaaaaaatgcttaaagcacttctaagtgagggtgaaagcatctgggagatcactgagaaaatactaaattcgtttgagtatacttcgagatttacaaaaacaaaaa ctttataccaattcctcttcctagctactttcatcaattgtggaagattcagcgatattaagaacgttgatccgaaatcatttaaattagtccaaaataagtatctgggagtaataatccagt gtttagtgacagagacaaagacaagcgttagtaggcacatatacttccttagcgcaaggggtaggatcgatccacttgtatatttggatgaattttgaggaattctgaaccagtccta aaacgagtaaataggaccggcaattcttcaagcaataaacaggaataccaattattaaaagataacttagtcagatcgtacaataaagctttgaagaaaaatgcgccttattcaatc tttgctataaaaaatggcccaaaatctcacattggaagacatttgatgacctcatttctttcaatgaagggcctaacggagttgactaatgttgtgggaaattggagcgataagcgtg cttctgccgtggccaggacaacgtatactcatcagataacagcaatacctgatcactacttcgcactagtttctcggtactatgcatatgatccaatatcaaaggaaatgatagcat tgaaggatgagactaatccaattgaggagtggcagcatatagaacagctaaagggtagtgctgaaggaagcatacgatacccccgcatggaatgggataatatcacaggaggt actagactacctttcatcctacataaatagacgcata.

Ss intronic MS2 Repeats

24 copies of the MS2 hairpin sequence were cloned into a HDR repair template in a PGem-T Easy backbone flanked by two ~1kb homology arm sequences from the *ss* locus. The reporter was integrated into the locus at this location: CTTACCACTTACCAGCTTGCCACC - 24xMS2 – GCTGACGATCCATCAATCTCCG. Pooled F1 siblings (~15 from each G0 x QBs cross, 16 G0 crosses screened in total) were screen by PCR to identify positive parents; in these cases, surviving siblings were crossed to balancers to establish lines, which were again screened by PCR to identify successful editing events. Junctions were confirmed via PCR and sequencing.

While it is formally possible that a different promoter might influence splicing dynamics and therefore the observed signal from an intronic reporter when making movies, we do not see signs of such differences in HCR *in situs* when comparing signal from intronic and exonic probes in the two backgrounds, such as non-spliced introns leaving the nucleus. Also, if splicing were faster or slower in the modified background, it is unlikely to be on the scale of minutes, which is how we measure off and on-intervals (with 30 or 60 second resolution).

R7 reporter pm181-mCherry

"PM181" is a previously identified regulatory region for the gene *sevenless*.[52,53] A larger region drives expression in several Seven-less-expressing PR types and a short region drives weaker, more specific expression in R7 PRs. This sequence was multimerized to

improve strength (four copies were used). To make a direct PM181-mCherry fusion, this four-copy sequence was cloned into the PBID-UASC[72] backbone from Addgene and integrated into landing site 86Fb on chromosome III.

PM181 consists of four repeats of this sequence: GGAAAAGGGGAAAGGAAATAATTACAATGAAAATGTGAAAGCATTTAGTATTT TATTTTGGTCACTTGGGAACGGAAGTTGCGGTGAGTTTGCGTGGGAAAAAGCTGAAGTCGTCACACATATATATGTGCATATATAAA ACAATATAGCAATGGCCATATAAAC.

In Situ Hybridization

In situ HCR 3.0 protocol was performed as described in Choi et al.[57] HCR hybridization probes and fluorescent amplifiers were designed by Molecular Instruments, Inc, or designed according to Wernet et al.[73]

Live Imaging

The movies shown in Figures 1E–1H; Videos S1 and S2; Figures 4C and 4D; Videos S4 and S5 were recorded with an OMX SR microscope. The movie shown in Figure 3B and Video S3 was recorded on a Zeiss 880 Confocal microscope using Fast-Airyscan at 1-minute time resolution. L3 eye-antennal discs were isolated from larvae and mounted in media adapted from Gallaghar et al.[74] and imaged *in vivo*. Tissues were incubated in SiR-DNA (Cytoskeleton. Inc., Cat. #CY-SC007), a live imaging DNA dye for tissue and nuclei localization, for 1 hour after dissection and prior to imaging in Figure 4C and Videos S4 and S5. Videos S1 and S2 were imaged at a 2-minute time resolution. Videos S4 and S5 were imaged at a 1-minute time resolution.

Controlling for MCP-GFP aggregation

MCP-GFP can form aggregates in some contexts. We demonstrate this is not the case: we show images where we drive the same (or higher) levels of MCP-GFP in cells that do not transcribe *ss* (as shown by HCR *in situ* hybridization) and do not see bright puncta in these cells. We also observed a subset of R7s in which bright puncta do not appear, imaged in the same movies and conditions as Ss-ON R7s. If the dots we see in cells that transcribe ss were aggregates, similar aggregates would also be present in other cells where MCP-GFP is present that do not transcribe *ss*.

QUANTIFICATION AND STATISTICAL ANALYSIS

Quantification and statistics of IHC tissue

Adult and pupal retinas were imaged using confocal microscopy. In adults, the number of Rh4+ cells versus the number of Rh3+ cells (R7 layer) or Rh5+ versus Rh6+ cells (R8 layer) was counted, and the ratio of Ss-ON ommatidia was determined. In the dorsal region of the eye, all cells coexpressing Rh4 and Rh3 were considered Ss-ON type, while R7s expressing only Rh3 were considered Ss-OFF.[64] In all cases, the percentage of Rh4+ (in R7s) or Rh6+ cells was compared between experimental and control genotype, with an unpaired two tailed t test used to determine significance. We used a threshold of $p=0.05$ to determine significance unless otherwise noted in the figure legend. In cases of multiple comparisons, the Bonferroni correction was applied.

Analysis of HCR *in situ* hybridization stains

Active transcription sites were detected using a machine learning classifier implemented in the ilastik software developed by Berg et al.[68] The classifier was trained and refined using manually labeled spots, then applied to all HCR datasets. To determine the number of active transcriptional loci along the A/P axis, 5 series of seven non-overlapping volumes (150 pixels in x and y, 15 pixels in z) were placed at various positions along the A/P axis starting from just before the morphogenetic furrow. The number of unique loci within each volume was counted and averaged with the 5 other measurements at the same A/P position.

Analysis of live MS2 movies

For Videos S1 and S2, and analysis presented in Figure 1D, detection and tracking of M on/off traces was done manually using "multi-point" tool from FIJI and reported in Data S1. Within each R7 cell that exhibited ss transcription, each on/off event of *ss* transcription was recorded. Detection of a GFP spot in consecutive time points was considered "on" or *ss*-transcribing, while the duration between two "on" periods was recorded as an "off" duration. A diagram and example of one cell is shown in Figure 1F. All individual on and off events are plotted in Figure 1D using ggplot. A Wilcoxon rank sum test with continuity correction was used to compare the ss-on-durations of both genotypes and yields a p-value of 6.938e-06. The same data was then grouped by cell, where each data point in Figure 1E represents one cell and displays the percentage of the observation time a particular cell was "on" or transcribing *ss.* A Wilcoxon rank sum test with continuity correction was used to compare both genotypes and yields a p value of 0.00752.

For Videos S4 and S5, and analysis Figure 4D, detection and tracking of MS2 time traces was done using "quot," a simple GUI to compare detection and spot tracking methods. Spot detection was done via a ratio test where the likelihood of a Gaussian spot in the center of the subwindow is compared to the likelihood of a flat background with Gaussian noise. Parameters controlling the Gaussian kernel size, the subwindow size, and spot detection threshold were adjusted until a satisfactory detection accuracy was reached. The same parameter values were used to analyze all MS2 movies. The detected spots were connected into trajectories that tracked the locus in time. A spot detected in two consecutive time points would form a trajectory if the position in the later time point was within 5 um of the original detection. Spots were stitched together into trajectories using the 'conservative' tracking method where all trajectory assignments were unambiguous (i.e., no more than one detected spot within the search radius).

Current Biology
Article

 CellPress

Statistical tests of ON and OFF period distributions

Under a Poisson process, OFF times are exponentially distributed. In this situation, there is a constant probability of an event happening in each unit of time. For each genotype, we used a Bayesian grid approximation to estimate the posterior distribution for the probability that a cell in an OFF state would turn ON, given the data and the assumption of a Poisson process. Since our observations are at discrete one-minute intervals, we modeled this using a geometric distribution, the discrete analog of the exponential. From these posterior distributions we generated posteriors for the expected counts at each duration. 95% highest density intervals and the medians of these posteriors are shown in Figure 4D. To assess whether the actual data were consistent with the model, we performed a posterior predictive check by simulating 10,000 datasets from the posterior for each genotype, calculating a chi-square statistic comparing the simulated data to the theoretical expectation, and counting the fraction of times that the statistic from the simulated data exceeded that of the actual data.

We used a permutation approach to directly test whether the distribution of off-durations for *ss-snail* was more skewed than that of WT, with a longer right tail. Under the null hypothesis, the WT and *ss-snail* data are drawn from the same distribution, and so we generated a null distribution for the difference in skewness by randomly assigning one of the two genotypes to each datapoint, calculating the difference in skewness statistics ($skew_{ss-snail} - skew_{WT}$) for this scrambled dataset, and repeating this 10,000 times. The p-value is the fraction of times that the difference from the null distribution exceeds the difference in skewness for the actual data.

Relevant code used to run these tests can be found at: https://github.com/Yzhao4707/Ss_Dynamics.

Supplemental Information

Cell fate ratios are encoded by transcriptional

dynamics in the *Drosophila* retina

Julia Ainsworth, Yunchong Zhao, Ke Gao, Nicholas M. Gravina, Zachary H. Goldberg, Coleman Pinkerton, Scott A. Rifkin, Andreas M. Ernst, Hernan G. Garcia, and Michael W. Perry
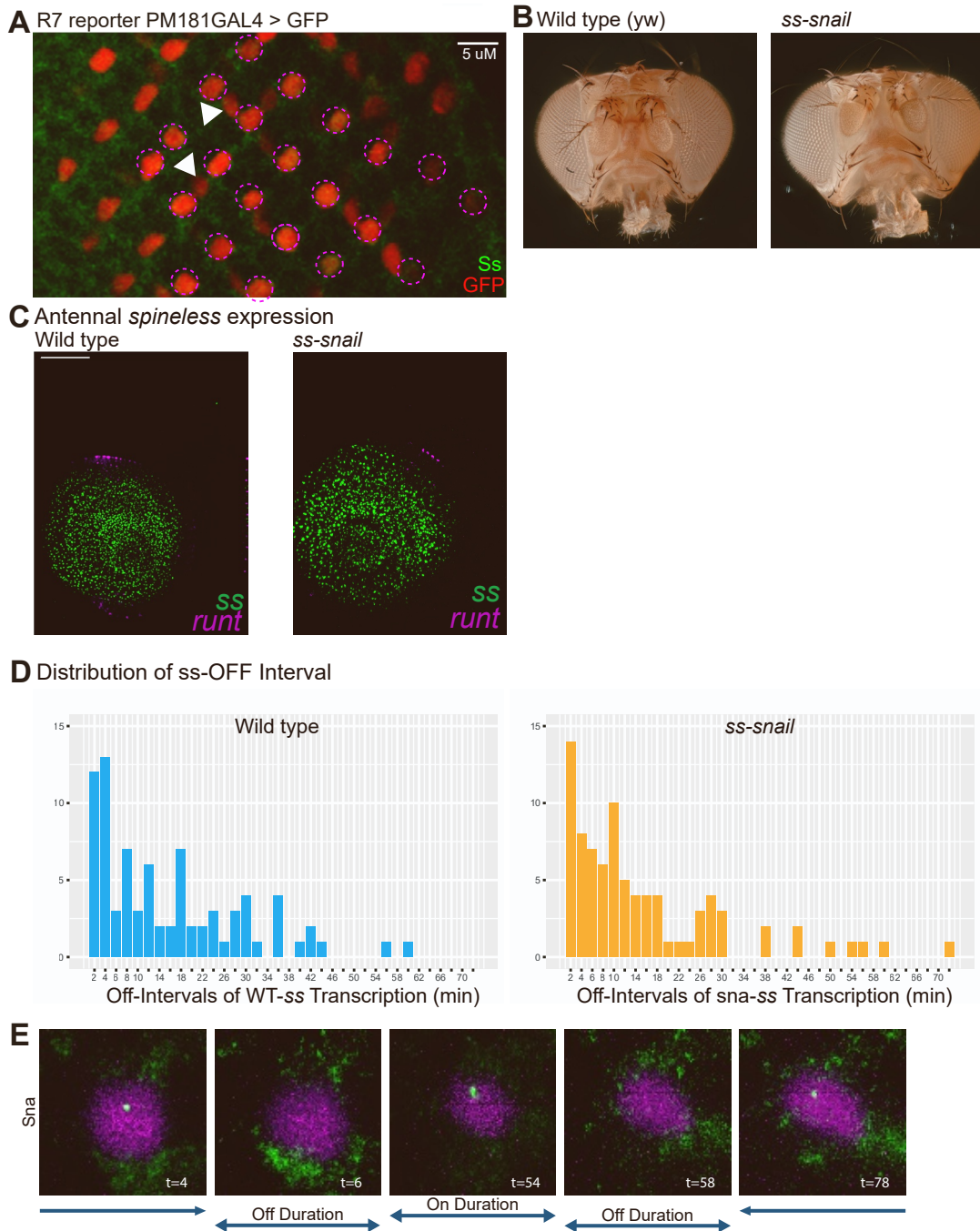
Figure S1. Confocal images and quantification. Related to Figure 1.

(A) FIHC showing an L3 eye disc with the fusion PM181-GAL4 driving GFP, which marks R7s (red) as well as some cone cells (identified with arrowheads in white). GFP and position were used to identify R7s (dashed magenta circles) for Figure 1A. Scale bar, 5µm.

(B) Homozygous viable modifications of the ss core promoter did not result in antennal defects in ss-snail core promoter (right) as compared with WT yw flies (left). Images taken at a distance of 5 uM and stacked with Zerene stacker software.

(C) HCR stain for spineless expression (green) in the antennal disc is comparable in WT ss core promoter with MS2 loops (left) or ss-snail (right). runt is the counterstain in magenta. Scale bar, 50µm.

(D) Distribution of Ss-OFF intervals (minutes) in WT (left panel, n = 90) and ss-snail (right panel, n = 96) backgrounds. Wilcoxon rank sum test with continuity correction; p-value = 0.6921

(E) Still frames of an example late L3 R7 turning ss ON/OFF at different time points of live imaging for ss-snail. Illustration below shows how on/off periods of ss were recorded. Time (t) refers to minutes elapsed since the movie began.
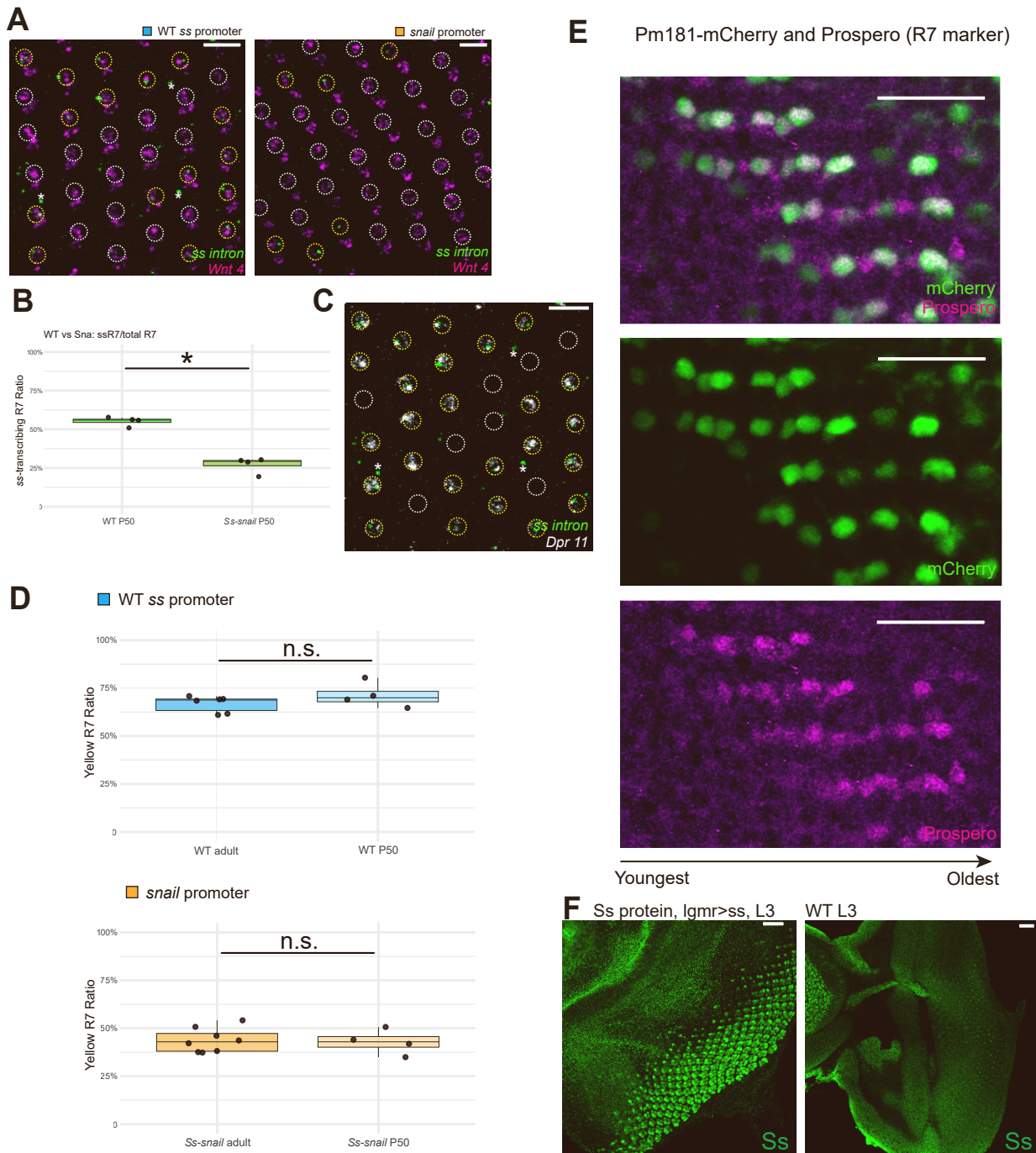
Figure S2. Confocal images and quantification. Related to Figure 2.

(A) HCR in situ hybridization of WT and ss-snail retina at P50. Wnt 4, ventral R7&R8 marker. Yellow dashed circles indicate R7s with active sites of ss transcription while white circles indicate inactive R7s. Asterisks, cone cell ss transcription. Scale bar, 10µm.

(B) Box plot comparing ss-transcribing R7 ratio between the WT and ss-snail at P50, Wilcoxon rank-sum test, p=0.0143.

(C) HCR in situ hybridization of P50 retina. dpr11 is downstream of Ss and labels a subset of R7 cells (yellow dashed circles) that will express Rh4 in adult stage; a subset of dpr11 R7s are actively transcribing ss. dpr11-negative R7s do not transcribe ss. Scale bar, 10µm.

(D) Box plot comparing yellow R7 ratio within the WT genotype (left) and the ss-snail genotype (right). Yellow R7s are Ss-positive R7s that are labeled by dpr11 at P50 and Rh4 at adult stages. Wilcoxon rank-sum test, WT, p=0.352; ss-sna, p=0.808.

(E) Larval eye disc showing the PM181-mCherry construct stained for mCherry (green) and Prospero (magenta). Prospero is a marker for R7s which turns on at around the same time as PM181-mCherry. Scale bar, 20µm.

(F) Left: UAS-Ss (green) is driven at high levels in all PRs by lGMR-Gal4 during larval development. Right: WT eye disc at same developmental stage for comparison. Scale bars, 20µm.
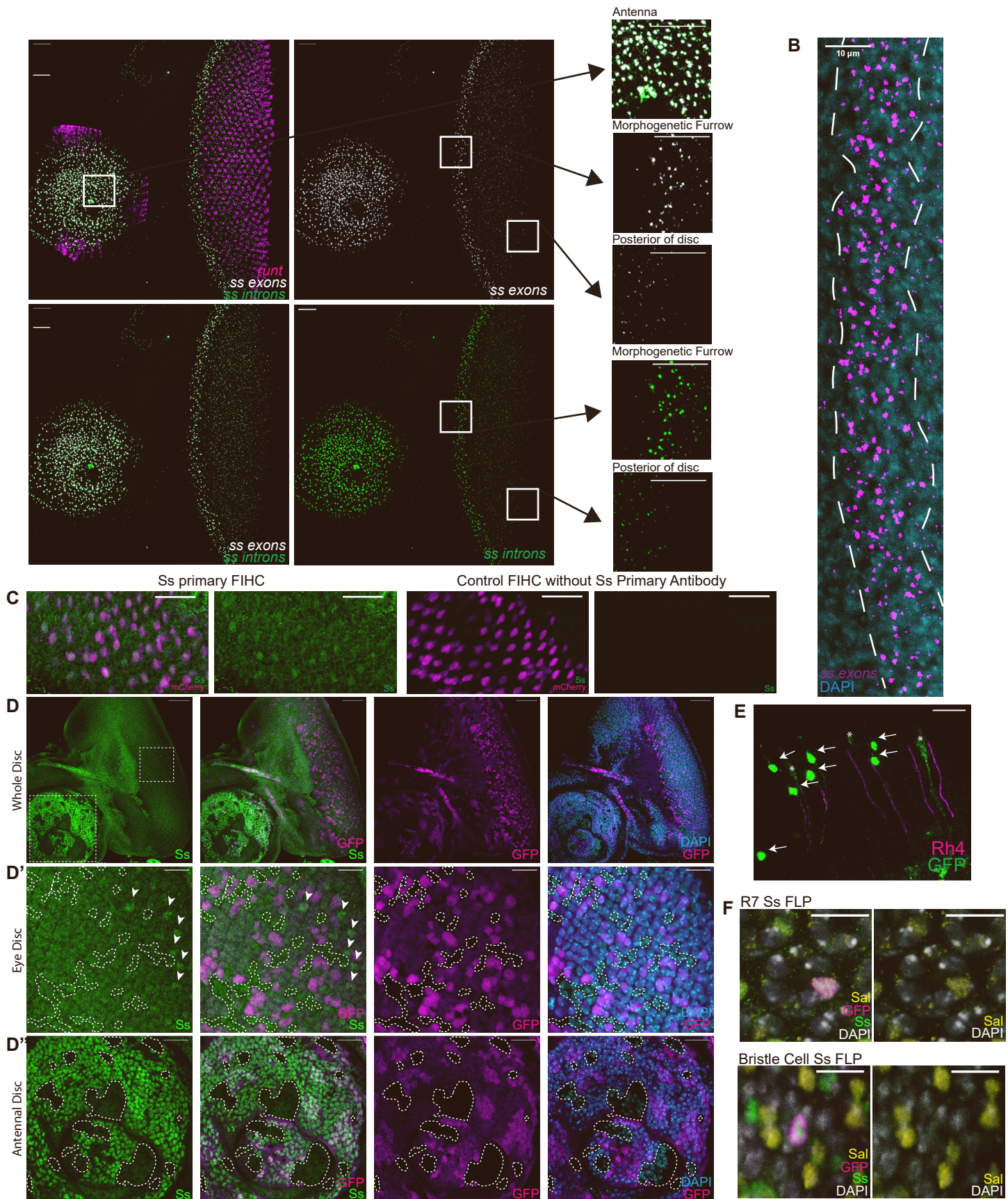
Figure S3. Confocal images. Related to Figure 3.

(A) The HCR in situ image shown in Figure 3E is displayed in more detail, including an additional channel and zoomed-in views. Confocal image shows a larval eye antennal disc with runt (R7 and R8 marker) mRNA in magenta and ss intronic mRNA in green. HCR probes against ss exons are included in gray. Larger views of regions near the Morphogenic Furrow (MF) and further posterior are shown for ss exons (top) and ss introns (bottom). A zoomed-in view of the antennal region is included to allow comparison of strong ss expression in the antenna to expression in the eye disc. Scale bar, 20μm.

(B) Close-up of ss transcription posterior of the MF in the stripe pattern. Scale bar, 10μm.

(C) A control no primary Ss antibody stain in the eye antennal disc showing two discs from the same genotype (PM181-mCherry) with R7s and many cone cells marked in magenta (mCherry) and the Ss antibody in green. The discs were dissected at the same time and imaged in parallel with the same laser settings. Background is high in the stain with antibody (left) and very low in the stain without primary antibody (right), but Ss can be seen in some R7 nuclei on the left (below) and not on the right (below). Scale bar, 20μm.

(D) An FRT-bearing chromosome with a Ss null mutation, with heat shock FLP in the background, was exposed to 37 degrees for 30 minutes at L1 stages, and dissected at late L3. Negative clones lacking ubi-GFP (in magenta) label cells homozygous for the Ss deletion. The cells without functional Ss protein still demonstrate nonspecific background from the Ss antibody (in green). Dashed square insets show zoomed in regions of clones in the eye disc (D') and antenna (D"). White dashed circles indicate clones that are GFP(-) and Ss (-). Arrowheads, Ss-positive R7s. Scale bars, 40μm, 10μm, 20μm respectively.

(E) FIHC of an adult Ss-FLP retina showing GFP (green) permanently genetically labeled cells which previously expressed Ss. Rh4 (magenta) shows R7s which expressed Ss during development. As evidence that Ss-FLP is functional, we observed a high number of GFP-positive clones in the antennal disc, where Ss is highly expressed (Figure 3G right). The most frequent labeling in the eye disc occurred in cells previously referred to as "bristle cells", which express Ss at high levels during pupal stages (Figure 3G middle, S3F right). By examining adult retinas, these cells become bristle neurons and not the bristle cell itself, as GFP-marked cells in adults have axons extending toward the brain (arrows). There were less frequent labeling of R7 PRs (Figure 3G, S3F left), which express Ss at relatively low levels even in Ss-ON R7s, and rare cases of labeled cone cells (asterisk). Cone cells exhibit low levels of "leaky" transcription of ss in movies (Videos 1-3, Figure 3B, arrow). We did not observe GFP labeling of any outer photoreceptors, R8 PRs, or pigment cells (15 discs, >9000 outer PRs). Scale bar, 20μm.

(F) Mid-pupal retina antibody stain for Ss (green), GFP (magenta), Sal (yellow) and DAPI (grey). Sal was used to identify R7s for Figure 3G. Scale bar, 10μm.
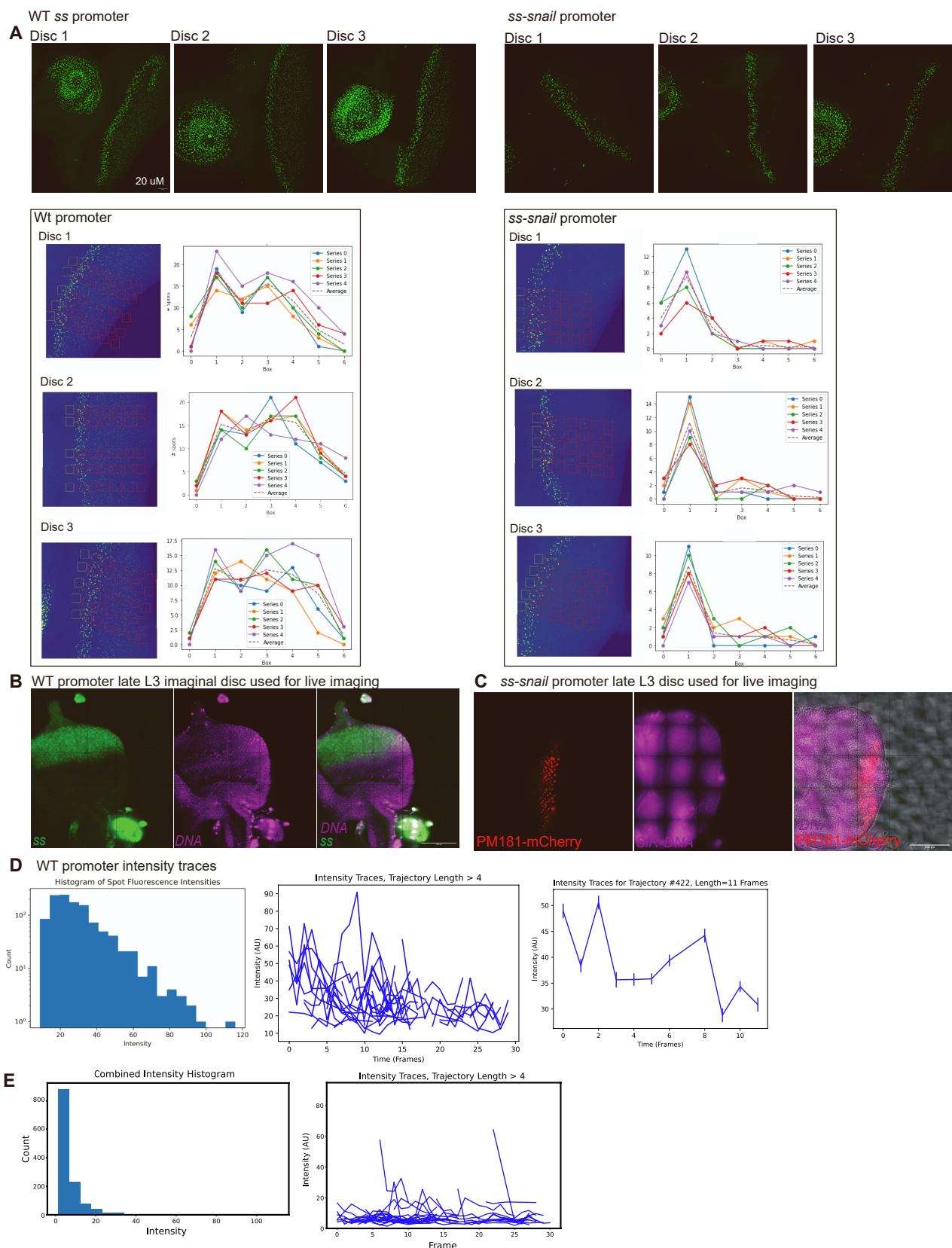
Figure S4. Confocal images and quantification. Related to Figure 4.

(A) Heat maps were generated from confocal images; the maximum-projections of confocal images used are shown at top. These heat maps were used in the process of quantifying the number of sites of active ss transcription across the anterior-posterior axis in fixed-tissue L3 eye imaginal discs, with WT ss promoter (n=3), left, compared to the ss-snail (n=3), right. Sites of transcription were quantified within red boxes (shown) at seven anterior-posterior positions, in A-P "series" at five positions on the dorsal-ventral axis. The number of sites of transcription counted within each box are plotted for each anterior-to-posterior series. Average counts by position for each disc are plotted below.

(B) Zoomed-out image of the eye disc shown in Figure 4C, at top, for perspective, taken before recording a movie of transcription. Data from this sample is included in the quantification shown in Figure 4D. Genotype: WT ss promoter. Green is MCP-GFP, magenta is SiR-DNA, a dye used to visualize all nuclei.

(C) Zoomed-out image of the eye disc shown in Figure 4C, at bottom, for perspective, taken before recording a movie of transcription. Data from this sample is included in the quantification shown in Figure 4D. Genotype: snail promoter, ss-snail. Magenta is SiR-DNA, a dye used to visualize all nuclei, and red is PM181-mCherry marking R7 PRs.

(D-E) Histogram of Spot Fluorescence Intensities and Intensity Traces in WT ss (D) and ss-snail (E) from live imaging analysis of Figure 4C. AU, artificial unit.
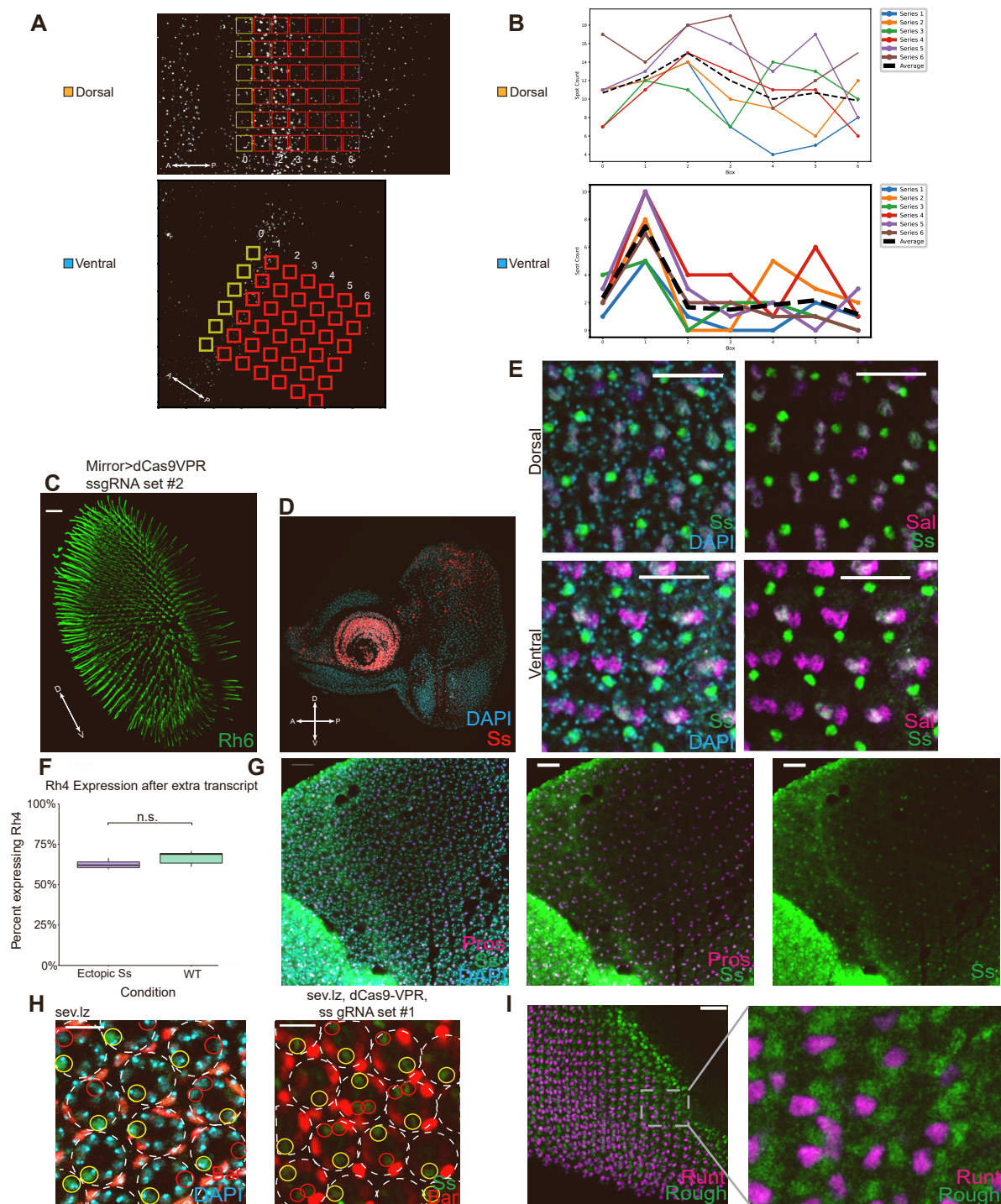
Figure S5. Confocal images and quantification. Related to figure 5.

(A) Heat maps of HCR in situ hybridization signal in L3 eye discs labeled with probes targeting intronic ss mRNAs. Signal shows sites of active transcription in ventral (control) vs. dorsal region of Mirr>d-Cas9-VPR, promoter-gRNA Set1. Sites of transcription within marked red squares are quantified at seven positions on the A/P axis in (B).

(B) Line graphs that show the number of sites of active transcription at positions on the A/P axis in ventral (control) vs. dorsal (Mirr-Gal4>UAS-dCas9-VPR, Ss promoter-gRNA Set1).

(C) An independent set of guides (promoter guide set #2, listed in Table S5) produced the same

effect as guide set #1 (Figure 5A,B) in flies where MirrorGAL4 drove expression of dCas9-VPR. The dorsal half of the retina was converted to Ss-ON type as assessed by Rh staining. Rh6 R8 cells (in green) are uniform in the dorsal half of the retina and stochastic in the ventral half. Scale bar, 20µm.

(D) L3 retina disc of Mirr>dCas9-VPR, ss-gRNA-set1. Overexpression of Ss protein can be seen in the entire dorsal half when compared to ventral half or WT (Figure 3D).

(E) At P50 we observed no ectopic expression in dorsal retina cell types despite a shift to a 100% R7 Ss-ON ratio in the Mirror>dCas9-VPR flies. Note the many cells other than R7 PRs marked by DAPI but not such as PRs R1-6, R8, pigment cells, and cone cells that do now express Ss (shown in green). Scale bar, 20µm.

(F) Adult Rh4 ratio of flies with the driver wGMR-GAL4 driving expression of ectopic Ss, with lGMR-GAL80 to suppress expression of the GAL4 protein in differentiated PRs. Purple represents the experimental genotype, while green represents wild type ss promoter used throughout the paper. N= 4 retinas and 1022 ommatidia for the experimental group and n = 6 retinas and 1439 ommatidia for the control group, p = 0.1131 (not significant) with a two-tailed independent t-test.

(G) Zoomed out view of a sev.lz P50 retina, used to quantify Ss expression in a larger number of ectopic R7s than the ones shown in Figure 5E. Scale bar, 20µm.

(H) Bar was used to identify the "true" R7 and the ectopic R7s in the sev.lz background (left) and mirr>d-Cas9-VPR with spineless promoter guide pair #1 (right). Bar is expressed at high levels in primary pigment cells and lower levels in R1/6, which flank the true R7.

(I) In sev.lz L3 eye discs many R3 and R4 cells are converted to R7-type PRs. This image shows expression of both Rough (R3/4 marker) and Runt (R7/R8 marker) in R3/4 PRs in the process of becoming R7-type PRs. Scale bar, 20µm.

A wGMR-GAL4>UAS-dCas9-CBP, Ss Promoter Guides #1 — Ss

B *spineless* transcript — DAPI / *ss exon* / *ss intron*
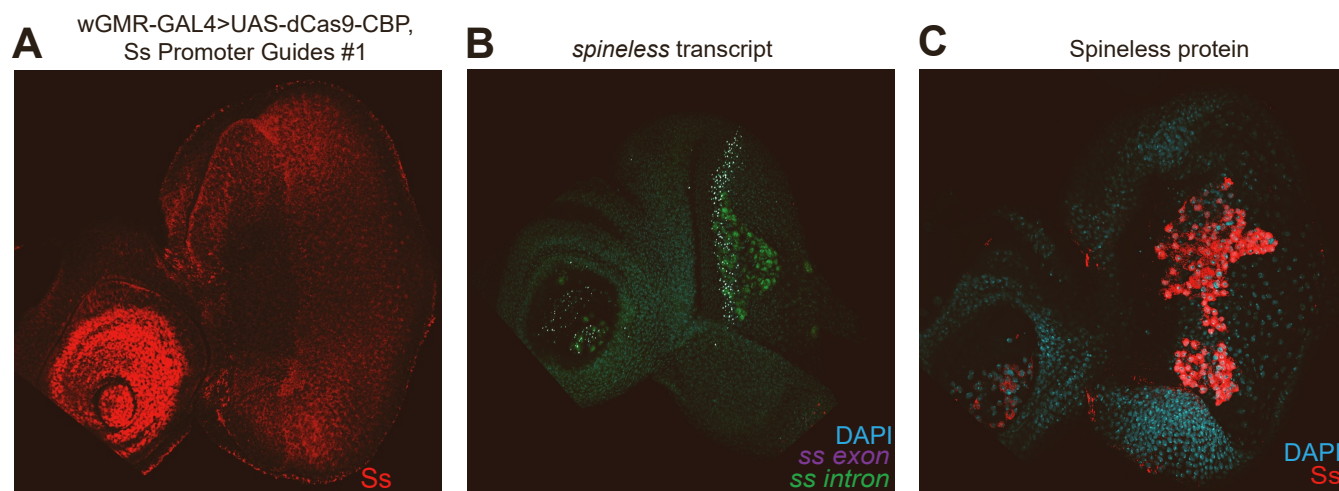
C Spineless protein — DAPI / Ss

Figure S6. Confocal images. Related to Figure 6.
(A) Targeting dCas9-CBP to the ss locus does not ectopically drive Ss expression in cells that do not normally express Ss, suggesting that it is still adequately repressed in many cell types. This provides additional evidence that CBP is not a general transcriptional activator, unlike VPR (Figure S5D). Image was over-saturated on purpose to show weak R7 Ss expression. Strong Ss expression can be seen in the antennal disc. We did not observe ectopic Ss expression anterior of specified R7s or in non-R7 cell types (outers, R8, cone cells, etc.).
(B-C) In the dCas9-CBP background, with gRNA targeting the ss promoter, some cells delaminate from the eye antennal disc and express high levels of spineless transcript (S6B, green) and protein (S6C, red). This may be due to leaky Ss expression ahead of or in the MF or may be a non-specific effect of CBP overexpression.

Gene	Sequence
Ss promoter (replaced)	TGGCCAGTGTGTTCCGCCAGGACTGGTTTTTCCATTCGTTT CGTGGCGCCGCTCAGTTCTTGTTGGAATCTCAAAGCGTTTA CGTGGCCGCAGCGCAGCAGAGTCACGTTTGAAAGAGTGC GAGTGAGAGATAGCGACTTAGAGCACCGCGCCG
Snail promoter (inserted)	GACAGCGGCGTCGGCAGAGGCGCAGAGTTCCGGGTATAA AAGAGCGTGCTCGACTGTTGACCTGTCACAGCCACCTCAG CTCTCGTTGAGAACGCAACCA

Table S1. Swapped sequences. Related to Figures 1,3, and 4.

Figure	Genotype
Figure 1A	L3: PM181GAL4, GAL80ts/Sp or CyO; pm181mcherry/UAS-GFPnls
	P50: yw122; sp/CyO; ss-24xMS2
	Adult: Ss promoter guides #1; dCas9VPR/MirrorGAL4
Figure 1C	Top: UAS-MCP-GFP/wGMR-GAL4; ss-24xMS2/pm181mcherry Bottom: UAS-MCP-GFP/wGMR-GAL4; ss-sna-24xMS2/pm181mcherry
Figure 1F	UAS-MCP-GFP/wGMR-GAL4; ss-24xMS2/pm181mcherry
Figure 1G	sp/CyO; ss-24xms2
	sp/CyO; ss-sna-24xms2
Figure 2B	**Left**: pm181GAL4, GAL80ts/UAS-Ss; pm181mcherry **Right**: same genotype, temperature shifted
Figure 2F	Left: UAS-Ss Right: GAL4-ey, UAS-flp/sp or CyO; FRT82b gmrhid/FRT82b SsDel115.7
Figure 2G	Left: sp/CyO; ss-24xms2 Right: GAL4-ey, UAS-flp/sp or CyO; FRT82b gmrhid/FRT82b SsDel115.7
Figure 3B	wGMR-GAL4/UAS-MCP-GFP ;PM181mcherry/ ss-24xms2
Figure 3D	PM181GAL4,GAL80ts/sp or CyO; PM181mcherry/UAS-GFPnls
Figure 3E	Sp/CyO; ss-24xms2
Figure 3G	Ss-flp/ubiFRT-stop-Stinger
Figure 4A	Left: Sp/CyO; ss-24xms2 Right: Sp/CyO; ss-sna24xms2
Figure 4C	Top: UAS-MCP-GFP/wGMR-GAL4; ss-24xMS2/pm181mcherry Bottom: UAS-MCP-GFP/wGMR-GAL4; ss-sna-24xMS2/pm181-mCherry
Figure 5A-C	UAS-dCas9VPR/Ss promoter guides #1; Mirr-GAL4/lGMR-GAL80
Figure 5D	Sp/CyO; ss-24xms2
Figure 5E	yw, hsflp; sp/CyO; Sev.Lz/Tm2
Figure 5F	UAS-dCas9VPR/Ss promoter guides #1; Mirr-GAL4/Sev.Lz
Figure 6B	wGMR-GAL4/Ss Promoter Guides #1; UAS-dCas9-CBP

Table S2. Complete fly genotypes used in Figures 1-6. Related to Figures 1-6.

Supplemental Figure	Genotype	Source
Figure S1A	PM181GAL4, GAL80ts/Sp or CyO; pm181mcherry/UAS-GFPnls	PM181GAL4: [S1] PM181mcherry: this paper, UAS-GFPnls: BDSC 4775 GAL80ts: BDSC 7108
Figure S1B	yw	
	sp/CyO; ss-sna-24xms2	This paper
Figure S1C	sp/CyO; ss-24xms2	This paper
	sp/CyO; ss-sna-24xms2	This paper
Figure S1E	UAS-MCP-GFP/wGmr-GAL4; ss-sna-24xMS2/pm181mcherry	UAS-MCP-GFP: This paper
Figure S2A-D	sp/CyO; ss-24xms2 sp/CyO; ss-sna-24xms2	This paper
Figure S2E	PM181GAL4, GAL80ts/Sp or CyO; pm181mcherry/UAS-GFPnls	PM181GAL4: [S1] PM181mcherry: this paper, UAS-GFPnls: BDSC 4775 GAL80ts: BDSC 7108
Figure S2F	UAS-Ss;lGMR-GAL4	UAS-Ss: From Claude Desplan LGMR-GAL4: From Claude Desplan
Figure S3A-B	sp/CyO; ss-24xms2	This paper
Figure S3C	wGMR-GAL4, GAL80ts; pm181-mCherry	WGMR-GAL4: From Claude Desplan
Figure S3D	Hsflp/hsflp; sp/Cyo; FRT82b, ubigfp/FRT82b SsDel115.7	Ss mutant line from Mattias Wernet
Figure S3E-F	Ss-flp/ubiFRT-stop-Stinger	Ss-flp: This paper UbiFRT-stop-Stinger: [S2]
Figure S4A	Left: sp/CyO; ss-24xms2 Right: sp/CyO; ss-sna-24xms2	This paper
Figure S4B	UAS-MCP-GFP/wGMR-GAL4; ss-24xMS2/pm181mcherry	WGMR-GAL4: From Claude Desplan
Figure S4C	UAS-MCP-GFP/wGMR-GAL4; ss-sna-24xMS2/pm181-mCherry	WGMR-GAL4: From Claude Desplan
Figure S5A&B	UAS-dCas9VPR/Ss promoter guides #1; Mirr-GAL4/lGMR-GAL80	lGMR-GAL80: from Mattias Wernet
Figure S5C	UAS-dCas9VPR/Ss promoter guides #2; Mirr-GAL4/lGMR-GAL80	lGMR-GAL80: from Mattias Wernet
Figure S5D&E	UAS-dCas9VPR/Ss promoter guides #1; Mirr-GAL4/lGMR-GAL80	lGMR-GAL80: from Mattias Wernet
Figure S5F	Ectopic Ss: wGMR-GAL4/UAS-Ss; lGMR-GAL80	lGMR-GAL80: from Mattias Wernet

Figure S5G	yw, hsflp; sp/CyO; Sev.Lz/Tm2	Sev.lz: From Andrew Tomlinson
Figure S5H&I	Left: yw, hsflp; sp/CyO; Sev.Lz/Tm2 Right: UAS-dCas9VPR/Ss promoter guides #1; Mirr-GAL4/Sev.Lz	
Figure S6A-C	UAS-dCas9CBP; wGMR-GAL4, Ss promoter guides #1	

Table S3. Supplemental Fly genotypes, used in FiguresS1-6. Related to STAR Methods.

Name	Sequence
ss promoter guides #1.1 (5')	AAAGGGAGCGACCAACCAAGT
ss promoter guides #1.2 (5')	TATGGCGACGCTGGAACGGT
ss promoter guides #1.3 (5')	GCCCCCTATAACGAAACTAC
ss promoter guides #1.4 (5')	CGAGCGATCGCCAAGCGACG
ss promoter guides #2.1 (5')	CAGTCCTGGCGGAACACAC
ss promoter guides #2.2 (5')	ACGCCGCCCGCGTGTTCCA
ss promoter guides #2.3 (5')	CTCTCACTCGCACTCGGCG
ss promoter guides #2.4 (5')	AAACGAGGCACAAAGGCGA
ss early enhancer guides #1	AACGCATTCGTATGTAGCCCC
ss early enhancer guides #2	ACACGTCTAGCAAAAGTCAG
ss early enhancer guides #3	ATAATTGCGCCAAGAAACAG
ss early enhancer guides #4	TGGTCATCTCATTACCGTTG
ss late enhancer guides #1	ATCCCACCCTGCCCTCTACGG
ss late enhancer guides #2	TAAAATCCACCACCGAAGTG
ss late enhancer guides #3	GGCCAAAACATATGTCGCAG
ss late enhancer guides #4	AGCGATTCTAGGGGGAAGGA
ss flp guide #1	CAGCTGGCTCATTGCTAGGG
ss flp guide #2	GCCCTAGCAATGAGCCAGCT
Ss intronic ms2 repeat insertion guide #1	TTACCAGCTTGCCACCTTG
Ss intronic ms2 repeat insertion guide #2	TTGATGGATCGTCAGCGGG

Table S4. CRISPR gRNAs. Related to Figures 1-6.

Name	Sequence
757Ss5'int-leftHA-F1	atggtaccAACTCGCCTCTGGTTGCTCTGC
758Ss5'int-leftHA-R1	tgaccggtGGTGGCAAGCTGGTAAGTGGTAAG
759Ss5'int-rightHA-F1	atcccgggGCTGACGATCCATCAATCTCCG
760Ss5'int-rightHA-R1	cgaagcttAACGGAGCCGCTTGAAGCTAAGG

Table S5. Primers. Related to STAR Methods. Homology arm repair template for *ss-snail*.

Plasmid	Reference or Source
PCFD5	Port et al [S3]
pUC57	Addgene Plasmid #54338
pBluescript	Addgene #133885
pBID-UASC	Wang et al [S4]

Table S6. Plasmids. Related to STAR Methods.

Probe	Source
Ss introns	Molecular Instruments
Ss exons	Molecular Instruments
Runt	Molecular Instruments
Prospero	Molecular Instruments
Wnt4	Designed using tool provided in [S5], P50 ventral R7& R8 marker
Dpr11	Designed using tool provided in [S5], downstream of Ss.

Table S7. HCR Probes. Related to STAR Methods.

Supplemental References

S1.   Lee, C.H., Herman, T., Clandinin, T.R., Lee, R., and Zipursky, S.L. (2001). N-cadherin regulates target specificity in the Drosophila visual system. Neuron *30*, 437–450.

S2.   Evans, C.J., Olson, J.M., Ngo, K.T., Kim, E., Lee, N.E., Kuoy, E., Patananan, A.N., Sitz, D., Tran, P., Do, M.-T., et al. (2009). G-TRACE: rapid Gal4-based cell lineage analysis in Drosophila. Nat. Methods *6*, 603–605.

S3.   Port, F., and Bullock, S.L. (2016). Augmenting CRISPR applications in Drosophila with tRNA-flanked sgRNAs. Nat. Methods *13*, 852–854.

S4.   Wang, J.W., Beck, E.S., and McCabe, B.D. (2012). A modular toolset for recombination transgenesis and neurogenetic analysis of Drosophila. PLoS One *7*.

S5.   Kuehn, E., Clausen, D.S., Null, R.W., Metzger, B.M., Willis, A.D., and Özpolat, B.D. (2022). Segment number threshold determines juvenile onset of germline cluster expansion in Platynereis dumerilii. J. Exp. Zool. Part B Mol. Dev. Evol. *338*, 225–240.